

## INFORMATION TO USERS

This manuscript has been reproduced from the microfilm master. UMI films the text directly from the original or copy submitted. Thus, some thesis and dissertation copies are in typewriter face, while others may be from any type of computer printer.

**The quality of this reproduction is dependent upon the quality of the copy submitted.** Broken or indistinct print, colored or poor quality illustrations and photographs, print bleedthrough, substandard margins, and improper alignment can adversely affect reproduction.

In the unlikely event that the author did not send UMI a complete manuscript and there are missing pages, these will be noted. Also, if unauthorized copyright material had to be removed, a note will indicate the deletion.

Oversize materials (e.g., maps, drawings, charts) are reproduced by sectioning the original, beginning at the upper left-hand corner and continuing from left to right in equal sections with small overlaps. Each original is also photographed in one exposure and is included in reduced form at the back of the book.

Photographs included in the original manuscript have been reproduced xerographically in this copy. Higher quality 6" x 9" black and white photographic prints are available for any photographs or illustrations appearing in this copy for an additional charge. Contact UMI directly to order.

# UMI

A. Bell & Howell Information Company  
300 North Zeeb Road, Ann Arbor MI 48106-1346 USA  
313/761-4700 800/521-0600



THE 1993-'94 SURGE OF BERING GLACIER, ALASKA  
OBSERVED WITH SATELLITE SYNTHETIC APERTURE RADAR

A  
THESIS

Presented to the Faculty  
of the University of Alaska Fairbanks  
in Partial Fulfillment of the Requirements  
for the Degree of

MASTER OF SCIENCE

By  
James Joseph Roush, B.A.

Fairbanks, Alaska

May 1996

© 1996 James Joseph Roush

**UMI Number: 1379805**

**Copyright 1996 by  
Roush, James Joseph**

**All rights reserved.**

---

**UMI Microform 1379805  
Copyright 1996, by UMI Company. All rights reserved.**

**This microform edition is protected against unauthorized  
copying under Title 17, United States Code.**

---

**UMI**  
300 North Zeeb Road  
Ann Arbor, MI 48103

THE 1993-'94 SURGE OF BERING GLACIER, ALASKA  
OBSERVED WITH SATELLITE SYNTHETIC APERTURE RADAR

By  
James Joseph Roush

RECOMMENDED:

William D. Harrison

David N. Mann

Ray A. Johnson  
Advisory Committee Chair

Paul W. Layer  
Department Head, Geology and Geophysics

APPROVED:

Paul B. Beckwith  
Dean of the College of Natural Sciences

W. A. Kan  
Dean of the Graduate School

4-11-96  
Date

### Abstract

Sequential synthetic aperture radar (SAR) images acquired by the First European Remote Sensing Satellite (ERS-1) were employed for observation of the 1993-'94 surge of Bering Glacier, Alaska. Evidence of accelerated motion became visible in late April 1993. Subsequently the surge front propagated down-glacier at a mean velocity of 90 *m/day* between 19 May and 25 August, reaching most of the 34 *km* perimeter of the terminus by shortly after 25 August. The calving terminus then advanced rapidly into proglacial Vitus Lake at a maximum rate, during 9 August to 18 October, of 19*m/day* in its central area. The propagating surge front consisted of a distributed region of undulations and bulges on the glacier surface having heights, estimated from SAR data, of 40 to 110 *m* and widths varying from 0.7 to 1.5 *km*. The measurements were made using terrain-corrected, geocoded and coregistered images.

## Table of Contents

<b>Abstract</b> .....	iii
<b>List of Figures</b> .....	vi
<b>Acknowledgments</b> .....	viii
<b>Chapter 1 Introduction</b> .....	1
<b>Chapter 2 An Overview of Glacier Surging</b>	
2.1 Introduction.....	4
2.2 A Definition of Glacier Surging.....	4
2.3 Documented Surges and the Surge Mechanism.....	6
<b>Chapter 3 Bering Glacier: History and Pre-Surge Conditions</b>	
3.1 Introduction.....	10
3.2 Bering Glacier .....	10
3.3 Historical Observations.....	13
3.4 Current Research.....	14
3.5 Holocene History .....	16
3.6 Surge History .....	19
<b>Chapter 4 SAR Imaging</b>	
4.1 Introduction.....	23
4.2 SAR Principles.....	23
4.3 Image Errors.....	28
4.4 Applications .....	34
<b>Chapter 5 Image Processing</b>	
5.1 Introduction.....	38
5.1.1 Radiometric Calibration.....	38
5.1.2 Geocoding .....	38
5.1.3 Geometric Rectification .....	39
5.2 The Terrain Correction Algorithm.....	40
5.2.1 Preprocessing .....	41
5.2.2 DEM Processing .....	42
5.2.3 Simulation of the SAR Image .....	44
5.2.4 SAR Correlation.....	45
5.2.5 Geocoding and Geometric Correction .....	46
<b>Chapter 6 Image Analysis</b>	
6.1 Introduction.....	50
6.2 Measurement of Surge Propagation and Terminus Advance Rates.....	50

6.3 Measurement of Bulge Heights and Estimation of Ice Velocity.....	51
6.4 Computer Animation of Sequential Imagery .....	55
<b>Chapter 7 Results</b>	
7.1 Introduction.....	58
7.2 Observation in Sequential Imagery.....	58
7.3 Surge Front Propagation and Terminus Advance .....	70
7.4 Bulge Heights and Ice Velocity Estimates.....	76
7.5 Description of Computer Animation of Imagery.....	76
7.6 Discussion of Errors.....	77
<b>Chapter 8 Discussion</b>	
8.1 Introduction.....	78
8.2 Comparison With Other Surges .....	78
8.2.1 Size and Setting.....	79
8.2.2 Time of Surge Onset .....	80
8.2.3 Surge Propagation, Ice Velocity, and Terminus Advance .....	82
8.2.4 Surge Termination and Flooding .....	85
8.3 Surging Activity in 1995.....	87
<b>Chapter 9 Summary and Conclusions</b> .....	89
<b>References Cited</b> .....	94

## List of Figures

Figure	Page
3.1 The location of Bering Glacier.....	11
3.2 The geography of the lower reaches of Bering Glacier.....	17
4.1 Scanning configuration of a side looking SAR satellite .....	27
4.2 The slant range image projection.....	30
4.3 SAR image range distortion.....	30
4.4 Relative skew and scale errors .....	30
4.5 Image errors resulting from terrain changes .....	32
4.6 SAR image foreshortening.....	32
4.7 SAR image layover .....	33
4.8 SAR image shadowing.....	33
5.1 Phases of terrain correction.....	40
6.1 Bulge height calculation from SAR derived slope angles .....	54
6.2 Continuity equation for estimation of ice velocity.....	56
7.1 SAR image of Bering Glacier on November 22, 1992 .....	59
7.2 SAR image of Bering Glacier on March 26, 1993.....	61
7.3 SAR of Bering Glacier on April 30, 1993 .....	62
7.4 SAR of Bering Glacier on June 23, 1993.....	64
7.5 SAR image of Bering Glacier on August 9, 1993.....	66
7.6 SAR image of Bering Glacier on August 25, 1993.....	67
7.7 SAR image of Bering Glacier on September 13, 1993 .....	69

<b>Figure</b>	<b>Page</b>
7.8 SAR image of Bering Glacier on October 18, 1993 .....	71
7.9 Four sequential surge front positions overlayed on a SAR image.....	72
7.10 Plotted sequential positions of the surge front.....	73
7.11 Plotted sequential positions of the advancing terminus.....	75

## Acknowledgments

I would like to thank Dr. Craig S. Lingle for taking a chance on a student without a geophysical background, and providing me with an opportunity to do truly innovative and exciting research. His input, ideas, and guidance made this project possible. Thanks also to my advisory committee members Dr. William D. Harrison and Dr. Daniel H. Mann. Their input at key points during this project helped to keep me on track and to not lose sight of the larger questions addressed by this thesis. Thanks to Dr. Shusun Li for help with SAR image analysis methods and to Mr. Kenneson G. Dean for serving as an examiner at my thesis defense.

Special thanks go to Mr. Richard M. Guritz for being involved in my thesis project at almost every stage, for introducing me to high performance computing, and for all those late night work sessions. His assistance made every aspect of this project possible. The image processing and analysis that form the basis of this thesis were carried out on the Interactive Image Analysis System (IIAS) of the Alaska SAR Facility, and the visualization workstations of the Arctic Region Supercomputing Center.

Thank you to those who provided financial support for my studies, including the Department of Geology and Geophysics (University of Alaska Fairbanks) for a teaching assistantship, and NASA (grant NAGW-2827, NRA 91-0SSA-07), the Alaska Space Grant Program, and the Arctic Region Supercomputing Center for funding my research assistantship at various times. Thanks also to the Geophysical Institute, University of Alaska Fairbanks, for providing first class facilities and a wonderful working

environment. Thank you to the Alaska Quaternary Center and to the Center for Global Change and Arctic System Research for various small grants.

I would like to thank Mr. Austin Post for taking an interest in my work and thereby providing great inspiration. I am honored to be associated with such an accomplished scientist. Great appreciation goes also to Dr. Bruce F. Molnia for welcoming me into his projects at Bering Glacier and for making available the valuable resources at his disposal. My extraordinary experiences in the field were made possible by him. Thank you Ms. Kimberly Lohuis for helping me so much and for working so hard and in the field at Bering Glacier. Thanks to everyone at Fishing and Flying air charter service in Cordova, Alaska, and to Ron Carlson for being the best helicopter pilot a glaciologist could ever want.

Finally I would like to thank the people who have provided support and inspiration and have helped to get me here, including: John McGuire of Charlotte Public High School, Charlotte, Michigan for giving me my first taste of earth science and providing me with a direction; the faculty of the Department of Geology at Albion College, Albion, Michigan, especially Dr. Lawrence Taylor for sparking my interest in glaciers; and most importantly my family. My dog Gus has been a loyal friend and companion throughout. My brother Wade has been an example and an inspiration. And finally, my parents Paul and Patricia have enabled me to do all of this work by always providing love and support. Thank you.

## Chapter 1: Introduction

Bering Glacier is North America's largest temperate latitude glacier, and largest surge-type glacier (Post, 1969). It has been observed to surge once approximately every 20 years in this century (Molnia and Post, 1995). The 20th century record of its surge behavior began with the aerial photographs of Bradford Washburn in 1938 (Molnia and Post, 1995), and has been continued by the U.S. Geological Survey using aerial photography, dendrochronology, and glacial geology and geomorphology (Molnia and Post, 1995). The most recent surge began in the spring of 1993 and lasted until the summer of 1995. Two pulses of fast ice motion occurred. The first ended in August of 1994. The second began in the spring of 1995, and lasted until late that summer (S. Raney, charter pilot, personal communication). Twenty-six years elapsed after the end of the last surge in 1967, and during that time the terminus of Bering Glacier retreated nearly 12 *km* (Molnia and Post, 1995). The two surge-pulses, between 1993 and 1995, readvanced the Bering Glacier terminus approximately 8 *km* (B. Molnia, of U.S. Geological Survey, personal communication). The once open proglacial Vitus Lake was transformed into a muddy iceberg-choked body of water bearing little resemblance to the lake of just one year before.

All of these catastrophic changes are "normal" for surge-type glaciers. Bering Glacier is one of over 200 glaciers in northwest North America which undergo periodic episodes of fast ice motion called surges (Post, 1969). Surges can and do radically alter the landscape on and around these glaciers. Advances of glacier termini and surge-ending

outburst floods are common and often effect changes in hydrologic systems or threaten the constructions of man. The Black Rapids Glacier in the central Alaska Range was nicknamed the "galloping glacier" when its 1936-'37 surge threatened to destroy both a nearby lodge and the Richardson Highway, which was, at that time, Fairbanks, Alaska's only road connection to the outside world (Heinrichs and others, 1995; Heinrichs and others, in press). Today the Trans-Alaskan oil pipeline parallels the Richardson Highway, and could be in the path of the Black Rapids Glacier if the magnitude of the next surge were to greatly exceed that of 1936-'37, as have past surges (Heinrichs and others, 1995; Heinrichs and others, in press).

The surging behavior of glaciers does not appear to be linked with climate change. Many glaciers which surge seem to do so with recurrence intervals ranging from 10 to 100 years (Meier and Post, 1969). The intervening periods are characterized by thinning and retreat of the lower glacier, accompanied by thickening of the upper glacier. The time interval between surges, as well as the grouping of surging glaciers in specific geographic regions suggest that specific conditions exist which control the timing of these events. As yet these conditions remain unknown (Clarke, 1986). More study of surging glaciers will be necessary before the phenomenon and its causes can be fully understood. There is, however, a hypothesis regarding the mechanism of fast ice motion during surges that is supported by detailed observations and measurements (Kamb and others, 1985) which may be applicable to most, if not all, surge-type glaciers including Bering Glacier. This mechanism involves the storage of basal water and fast sliding of a glacier on its bed.

Field studies of surging glaciers, however, tend not to be "easy" since most surge-type glaciers are located in remote mountain regions that are difficult and expensive to reach. For observation of large-scale surface changes during a surge, a viable alternative is the application of satellite synthetic aperture radar (SAR) imagery. The cost of studying a surge with satellite imagery is negligible compared to that of field research, and it enables year-round observation, as opposed to field study which is carried out, in general, during the summer. Use of SAR complements field study because it enables observation of entire glacier systems and allows the study of many events which might otherwise go unobserved. It is both a lack of sufficient observations of surging glaciers, combined with a lack of detailed analysis of these events, which has inhibited full understanding of this phenomenon. Spaceborne SAR will allow observation of a wider range of surging glaciers, and is thus likely to yield advances in comprehension of glacier surging.

This thesis is a study of the 1993-'94 phase of the recent Bering Glacier surge using SAR imagery from the First European Remote Sensing satellite (ERS-1). The images acquired, along with selected field data and observations, have been analyzed in order to partially characterize the event. The behavior of Bering Glacier during its surge is compared to the observed behavior of other surging glaciers.

## **Chapter 2: An Overview of Glacier Surging**

### ***2.1 Introduction***

An overview of the phenomenon of glacier surging is given. Surging is defined, and several well studied historical surge events are summarized. A summary of the current theory of glacier surging is given.

### ***2.2 A Definition of Glacier Surging***

A surging glacier is defined as one that alternates between brief periods of very rapid flow, lasting usually one to four years, and extended periods of quiescence which last 10 to 100 years (Kamb and others, 1985). During surge, a glacier can accelerate to velocities which are 10 to 100 times greater than normal, and then suddenly return to a normal state of flow (Kamb and others, 1985). Ice within a glacier can be displaced several kilometers or more during one surge event. Often this results in a dramatic advance of the terminus which has, at times, threatened human constructions (Heinrichs and others, 1995; Heinrichs and others, in press). This behavior seems not to be linked with climatic influences, a fact which must be considered when looking at glacier fluctuations for indications of climate change. An understanding of surging is, therefore, necessary for both scientific and engineering purposes.

This unusual phenomenon was first recorded in 1906 (Tarr, 1907 from Kamb and others, 1985) when a surge of the Variegated Glacier in Alaska's St. Elias Mountains was observed (Kamb and others, 1985). More recently, hundreds of surging glaciers have

been identified either by direct observation of a surge event, or by recognition of a characteristic "looping moraine" morphology on a glacier surface (Post, 1969).

The geographic distribution of surging glaciers is also an interesting aspect of the problem. Surge type glaciers have been identified in a number of climates from marine to continental, and in sub-polar to temperate thermal regimes (Post, 1969). This points to no obvious environmental control; yet surging glaciers seem to be grouped in specific geographic areas suggesting that such a control must exist. Many of the world's surging glaciers are located in Alaska and northwestern Canada, and within this region there are areas where surging glaciers are common and others where none exist. It is possible that tectonics and bedrock geology may influence the distribution of surging glaciers, as many are seen to lie over major fault systems and or on top of incompetent rock types (Harrison and others, 1994). However, there are glaciers which do not surge which are situated in similar regions.

Clarke (and others, 1986; 1991) showed statistically that surge-type glaciers tend to be longer than non-surge glaciers. They concluded that this factor is more consistent with the current theory of the cause of glacier surging, which involves failure of subglacial water drainage (Kamb and others, 1985), because longer glaciers have a higher probability of developing subglacial drainage problems (Clarke and others, 1986). This factor may be important for the Bering Glacier because of its extreme length.

### ***2.3 Documented Surges and the Surge Mechanism***

Light was shed on the mechanisms which enable fast glacier flow by the measurements of Kamb and others (1985) and Blankenship and others (1986). In the case of surging glaciers, this mechanism involves the failure of subglacial water drainage, which results in trapping and redistribution of water across the bed in a network of linked cavities (Kamb, 1987). This causes elevated subglacial water pressure which reduces friction, and causes accelerated basal sliding. First hypothesized by A. Post (unpublished), this mechanism was proven to operate during the 1982-1983 surge of Variegated Glacier, Alaska (Kamb and others, 1985). Since then evidence of this process has been seen during other surge events (Harrison and others, 1994).

When the Variegated Glacier surged in 1982 a number of researchers were ready to observe its progress (Kamb and others, 1985). Because the frequency of surge events at Variegated Glacier suggested a recurrence interval of 17 to 20 *years*, it was possible to survey the glacier thoroughly in its pre-surge condition so that its behavior during surge could be understood in the context of the entire cycle. Begun in 1973, the Variegated Glacier project culminated with the 1982-1983 surge when it was determined that a disruption of the basal water drainage network, accompanied by a transition to increased subglacial water storage and elevated subglacial water pressure, was indeed the process which initiated and sustained the surge (Kamb and others, 1985). A discharge of sediment laden water was seen to accompany each of several deceleration events, that last of which ended the surge.

The conclusions drawn from the Variegated Glacier surge were confirmed in a study of the 1987-'88 surge of the West Fork Glacier in the central Alaska Range (Harrison and others, 1994). The surge of West Fork Glacier occurred in one pulse which lasted 10 months and was seen to end with an increased discharge of sediment laden water. The similarities in speed, and the relationships between speed changes and sediment and water discharge, indicated that the mechanism of surging was the same as for both events (Harrison and others, 1994).

At least for Variegated Glacier and West Fork Glacier, this answers one of two main questions put forth by Raymond (1987), which was "what is the mechanism of fast motion during a surge?" Raymond's second question, "What initiates and terminates the fast motion? ", remains unanswered. The solution of this second problem may reveal why surging glaciers are located in specific geographic areas, and why they seem to surge with roughly consistent frequencies.

Medvezihy Glacier in the Pamirs of Asia has also been well studied. This is the only glacier to have been observed throughout an entire surge cycle (Dolgushin and Osipova, 1975). Medvezihy is a relatively small glacier ( $25 \text{ km}^2$ ) in which surges were observed in both 1963 and 1973. During the surge, some features common to most known surges were observed by Dolgushin and Osipova (1975). Fast flowing ice either reactivated or overrode stagnant ice downstream in the terminus. The active terminus advanced on a scale of kilometers at rates of 10 to 100 *m/day*. The surface elevation of the upper-glacier affected by the surge dropped up to 100 *m* and the terminus was thickened by 150 *m*. The volume decrease in the source area appeared roughly equal to

the volume increase in the receiving area. Also, the surge of Medvezihy was confined to the ablation area of the glacier below an icefall. It is not uncommon for a surge to occur wholly within the ablation area as the profile of the surging area seems to be more important than the total area of the glacier (Paterson, 1994). A break in slope will sometimes limit the extent of a surge.

In general, the behavior of Medvezhiy glacier during surge is characteristic of most surging glaciers. Fast flowing ice commonly moves downstream through stagnant ice, either reactivating it or flowing over it. These "waves" of fast ice have been seen to travel several times faster than the rate at which the ice is actually flowing, and they seem to propagate through glacier ice in a fashion similar to a wave moving through water where the individual particles are traveling at a fraction of the speed of the wave (Paterson, 1994). If the wave of fast ice, referred to as the surge front, reaches the terminus of a glacier, the glacier will advance. The 105 *m/day* rate of terminus advance at Medvezhiy Glacier is unusually high. However, many surging glaciers can advance their termini by several kilometers over a few months to a year. Also, not all surges reach the terminus and, although the glacier may not advance, the event is still considered a surge. In any surge a volume of ice is transferred from a reservoir area upstream to a receiving area downstream that may or may not extend to the terminus. This mass transfer is seen in the thinning of the reservoir area and the thickening of the lower reaches of a glacier. This radically alters the surface profile of a glacier and one control on the frequency of surges may involve the time needed for a glacier to return to a profile which is critical for surge onset (Paterson, 1994).

The velocity of the fast flowing ice in a surge is a primary indication of the type of ice flow that is taking place. Because surge velocities have been observed to be 10 to 100 times greater than normal rates of flow, it is presumed that basal sliding is the mechanism responsible for fast flow (Kamb and others, 1985). These abnormally high velocities typically cannot be produced by internal deformation alone. If accelerated basal sliding is the cause of rapid flow during surge, this suggests that friction is reduced by water storage which allows the glacier to slide rapidly, as indicated by Kamb and others (1985). Another possibility is that the bed of a surging glacier may deform enough to allow rapid sliding (Clarke, 1984; Blankenship and others, 1986; Alley and others, 1986). This differs from sliding caused by bed separation due to high subglacial water pressure.

The recognition of two possible mechanisms (hard bed versus soft bed) for basal sliding raises the important point that there may be no single cause or mechanism which can explain all surge events. Because surging glaciers exist in a number of climates and thermal regimes it seems reasonable to assume that there may be different types of surging in different regions, such as the long period, long duration surges of glaciers in Svalbard, versus the shorter, faster surges seen elsewhere (Dowdeswell and others, 1991). Our understanding of surging remains incomplete; study of many surges in different settings is likely to be required for full comprehension.

## Chapter 3: Bering Glacier: History and Pre-Surge Conditions

### 3.1 Introduction

The setting of Bering Glacier is described, and a brief review of the literature regarding the glacier and its Quaternary fluctuations is given. The behavior of the glacier prior to the onset of surging in 1993, as determined by Molnia and Post (1995), is outlined.

### 3.2 Bering Glacier

Bering Glacier is located in the Chugach Mountains of Southcentral Alaska. It is roughly 250 *km* east of Anchorage, midway between the communities of Cordova and Yakutat, Alaska. The glacier originates at a broad divide in the Bagely Icefield below the base of Mount St. Elias, at the Alaska/Canada border, and flows 185 *km* west and south to the Gulf of Alaska coast. Bering Glacier covers approximately 5200 *km*<sup>2</sup> and is generally considered to be the world's largest non-polar glacier. It joins with the smaller non-surging Steller Glacier on the coastal plain to form the Bering Glacier piedmont lobe (figure 3.1). The Steller Glacier is not considered in this study because it has not been observed to participate in surges of the Bering Glacier and is considered to be a separate and unique body of ice.

Bering Glacier is a temperate surging glacier which also has many of the distinguishing characteristics of a tidewater glacier (Molnia, 1993; Lingle and others,



1994). It terminates in a large proglacial body of water known as Vitus Lake. Vitus Lake is, depending on the current position of the glacier terminus, roughly 2-7 *km* wide and 15 *km* long (Molnia and Post, 1995). Vitus Lake and Bering Glacier are separated from the Gulf of Alaska by a narrow strip of glacial sediments and coastal deposits hereafter referred to as the Bering Glacier foreland, as stated in Molnia and Post (1995). The lake drains into the Gulf of Alaska via the Seal River, a short but large channel which carries all of the water discharged from Bering Glacier (Molnia and Post, 1995).

Bering Glacier is considered to be like a tidewater glacier because it is grounded well below sea level in its lower reaches (Molnia and others, 1990; Molnia 1993; Meier and Post, 1987). If the Bering Glacier foreland did not exist, the glacier would calve directly into the ocean and would no doubt display more of the characteristic instability of true tidewater glaciers. Unlike most tidewater glaciers, however, the Bering Glacier terminus before the recent surge was an ice surface which sloped down nearly to lake level before ending in a low ice cliff (Lingle and others, 1994). Icebergs which calved from the Bering terminus were seen to float significantly higher than the terminus. This indicated that the terminus was held below the level of hydrostatic equilibrium. Calving was, therefore, due probably to the bending stress resulting from upward pressure on the bottom structure, caused by ablation lowering the top surface below the level of hydrostatic equilibrium. Icebergs were seen to "pop up" after breaking away from the terminus (Lingle and others, 1994). This is the major difference from nonsurge-type tidewater glaciers, such as the Columbia Glacier, which has a high and active ice cliff at its terminus which calves because of fracturing at high rates of flow, causing ice to fall

away from the cliff as well as calve from below sea level. Also, most tidewater glaciers lose a large amount of mass annually due to calving. The Bering Glacier before surge appeared to be nearly stagnant, and most of its mass was lost due to ablation. The terminus retreated significantly during the 26 years following the last surge, receding as much as 10.7 km (Molnia and Post, 1995).

### ***3.3 Historical Observations***

Bering Glacier is named for the Danish explorer Vitus Bering who led the first European expedition to Alaska in 1728. The adjacent ice mass, the Steller Glacier, is named for George Steller, a German naturalist who accompanied Bering on his expeditions.

Observations of Bering Glacier were first recorded in 1837 by Captain Edward Belcher of the British Royal Navy (Pierce and Winslow, 1979). In his reports he describes seeing a ridge in profile that was composed of broken four sided pyramids of what appeared to be ice. Based on the position of his vessel it is clear that he was observing the Bering Glacier. His description of an elevated and broken ice mass visible from the Gulf of Alaska strongly suggests that he was observing the glacier in a state of surge (Muller et. al., unpublished).

The first map of the Bering Glacier terminus region was compiled by the U.S. Geological Survey (USGS) shortly after the turn of the century (Maddren, 1914). The first detailed map of the glacier was compiled in the 1950's by Don J. Miller of the USGS (Miller, 1961).

Aerial photographic observation was begun by Bradford Washburn in 1938. Photography was continued in the 1940's by the Army Air Force. In 1960 Austin Post began photographing glaciers in northwest North America for the University of Washington and continued his work for the USGS from 1964 through the early 1980's. Several hundred of Post's photographs cover the Bering Glacier during that period. Photography has been continued through the present by Robert Krimmel of the USGS. Field observations of Bering Glacier have been carried out by Bruce Molnia and others of the USGS from 1990 through the present (Molnia and Post, 1995).

### ***3.4 Current Research***

In addition to this project, a number of researchers have studied Bering Glacier during the 1990's. Both the USGS, and the State University of New York at Oneonta, with Syracuse University, have carried out continuing field projects at Bering Glacier prior to and throughout the 1993-'95 surge.

The USGS, under the direction of Bruce Molnia, has been studying the Bering Glacier foreland and the hydrologic system of Vitus Lake. Of principle interest before the surge was the rate of retreat of Bering Glacier, the amount of sedimentation in Vitus Lake, and the stability and rate of erosion of the foreland. The Bering Glacier, while surging periodically, has been in a general state of thinning and retreat throughout this century (Molnia and Post, 1995). It has been suggested that if the foreland were to erode away, Bering Glacier could become exposed to the relatively warm water of the Gulf of Alaska. Rapid retreat of the glacier might then occur and a large marine fjord system

could be created. While the likelihood of a breach in the foreland is not known, recent surge-related advances have probably not reversed the 20th century trend of volume loss due to ablation as noted by Molnia and Post (1995). During the recent surge the USGS continued its research and focused on the behavior and progression of Bering Glacier while surging.

The research group of Ernest Muller, Jay Fleisher, and others from Syracuse University and the State University of New York at Oneonta have focused on the glacial geologic history of the Bering Glacier along its eastern margin (Fleisher and others, 1990, 1994; Muller and Fleisher, 1995; Muller and others, unpublished). They have studied glacial activity in the vicinity of the smaller Tsvat and Tsiu Lake basins and have focused on reconstructing the Late Holocene fluctuations and surging history of the glacier as represented in the glacial geologic record.

Prior to the current research efforts at Bering Glacier, Austin Post published an important paper in which he explored the origins of folded medial moraines seen on the surface of the glacier (Post, 1972). Post determined that a repetitive pattern of folded moraines was the result of periodic surging within the glacier, and differential velocity between Bering Glacier and its tributaries during surge. Molnia and Post (1995) concluded that the total accumulation of folds in the medial zone between Bering and Steller Glaciers may represent at least five centuries of surging activity in Bering Glacier.

### ***3.5 Holocene History***

The primary reference for the Late Pleistocene and Holocene history of Bering Glacier is Molnia and Post (1995). The authors have synthesized a history of the glacier's fluctuations from the last glacial maximum to the present, from glacial geologic data. Their history is based on radiocarbon dating of peat, subfossil wood, and shells collected at the margins of Bering Glacier, and on dendrochronologic research conducted on the Bering Glacier foreland. The summary that follows is taken from their work, as it is the only published history to date.

Between 15,000 and 20,000 years before present (BP), Bering Glacier began to retreat from its last glacial maximum (LGM) position at the edge of the continental shelf in the Gulf of Alaska. Evidence of the glacier's extended position is seen in the Bering Glacier trough, a large submarine trough that extends from the coast in front of the present day glacier, out to the continental shelf break (Molnia and Post, 1995). Radiocarbon ( $C^{14}$ ) dating of organic peats adjacent to Bering Glacier, deposited on glacially eroded bedrock, mark the time of retreat at approximately 15,000 BP. Other  $C^{14}$  evidence suggests that the continental shelf was ice free by 10,000 BP and that the Bering Glacier had retreated into the Chugach mountains. If so, Steller Glacier would not have been a tributary and the present peidmont lobe would not have existed. There is no further evidence to indicate the extent of the glacier until about 8,000 BP.

Radiocarbon dates on peats formed adjacent to lateral moraines in the Hanna Lake area (See figure 3.2, adapted from Molnia and Post, 1995) suggest that the glacier has not

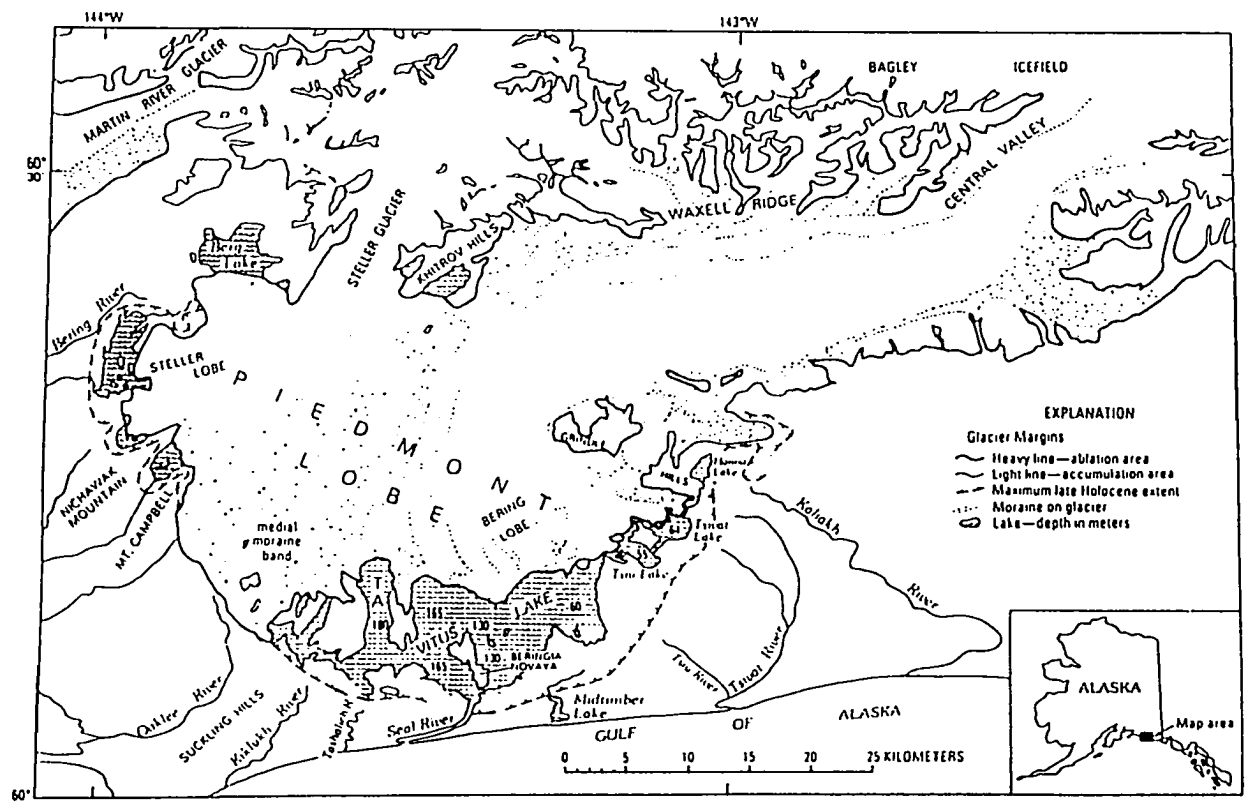


Figure 3.2 The geography of the lower reaches of Bering Glacier, adapted from Molnia and Post (1995). TA is Taslich Arm. Vitus Lake is shown in its pre-surge configuration.

expanded beyond the coastal plain since about 8,000 BP. This represents the glacier's late Holocene maximum position.

Radiocarbon dates of about 3,000 to 4,000 BP on clam shells found along the western margin of the Bering terminus, in Taslich Arm (figure 3.2) in 1993 indicate that the glacier was in a retreated position during the middle Holocene. The preserved clams are overlain by peat deposits dated at 3,000 BP (Molnia and Post, 1995) which suggests conditions favorable to abundant plant growth for a significant length of time, supporting the conclusion that Bering Glacier was retreated during this period. Overlying sand and gravel indicate that Bering Glacier then re-advanced to the vicinity of the Grindle Hills and deposition continued until about 2000 BP.

At this point in the stratigraphy of the foreland, a significant extended period of forest growth is indicated by the "Major Forest Bed" (MFB) seen by both Molnia and Post (1995), and Muller and others (1993, in progress). This forest bed consists of the preserved trunks of spruce and hemlock as old as 200 years in age and as large as 40 cm in diameter (Molnia and Post, 1995). This is an indication of a period of retreat of the Bering Glacier which lasted long enough for a major forest ecology to develop. Radiocarbon dates from around Vitus Lake suggest that this forest bed was in growth until about 1500 BP (Molnia and Post, 1995). The MFB was buried in up to 2 meters of silt, and subsequent re-growth occurred on the new surface immediately after burial. This new forest was then buried in 3 meters of silt and subsequently sheared off by an advance of the glacier. This occurred at about 1400 BP (Molnia and Post, 1995). The buried forest beds are overlain by up to 20 meters of outwash sand and gravel containing little or

no organic material. This suggests the Bering Glacier was active in the near vicinity for an extended period because no forest beds had time to develop within the sequence (Molnia and Post, 1995).

Forest growth near the terminus of Bering Glacier evidently resumed and continued until about 714 years BP, as indicated by the presence of large tree stumps buried in place by till and outwash (Molnia and Post, 1995). The till which overlies this forest bed is one of the few exposed tills anywhere in the foreland and it indicates a re-advance of the glacier to its neogacial maximum, nearly two kilometers beyond the largest buried trees (Molnia and Post, 1995). This position is seen as the neogacial maximum moraine which rims the foreland (figure 3.2). No forests of similar age have been able to develop on the Bering Glacier foreland since the neogacial maximum because periodic surging and the shifting of meltwater streams have destroyed forests before they could reach a similar maturity (Molnia and Post, 1995).

Trees standing on the maximum moraine date between 250 BP (according to dendrochronology) and the oldest living trees at 130 years BP (Molnia and Post, 1995). These dates indicate the recession from the maximum position began about 250 years ago. Recession since that time peaked at as much 12 km from the neogacial maximum moraine before the 1993 surge (Molnia and Post, 1995).

### ***3.6 Surge History***

Although the Bering Glacier has been in retreat throughout recorded history, the trend has been interrupted by several known surges (Molnia and Post, 1995). Evidence

for these surges exists in the form of relict folded moraines in the medial zone between the Bering and Steller Glaciers (Post, 1972). Historical observations (Pierce and Winslow, 1979), dendrochronologic records, interpretation of historical maps, field observation, and remotely sensed imagery show that surges also occurred in 1900, 1920, 1938-'40, 1957-'60, 1965-'67, 1993-'94, and 1995 (Molnia and Post, 1995; Lingle and others 1994; Fleisher and others, 1994; Roush and others, in press).

Aerial photographs indicate the 1965-'67 surge resulted in approximately 9 *km* of advance at the terminus, from which Bering Glacier was retreating and ablating until the 1993 onset of surging. The estimated total loss of surface area for the piedmont lobe of Bering Glacier in this century was 130 *km*<sup>2</sup> before 1993 (Molnia and Post, 1995). This indicates that periodic surging has been superimposed on the overall trend of retreat.

Evidence suggesting that periodic surging had taken place well before the last century may exist in the form of the tightly folded sets of medial moraines which make up the broad rock debris band (medial zone) between the Bering and Steller Glacier lobes of the piedmont lobe (Post, 1972). According to Post (1972), these "accordion folds" represent stretched medial moraine loops, which are "folded into" the medial zone by strong shear along the western margin of the main trunk of Bering Glacier during surges. That is, each successive surge creates a new set of accordion folds. Post (1972) interprets the total accumulation of folds in the medial zone to be a multi-century record of Bering Glacier's surges.

The record of historical surge events begins with the observations of Belcher in 1843 (Pierce and Winslow, 1979). The earliest 20th century evidence from USGS maps

of the Bering Glacier area (Martin, 1908; Maddren, 1914) do not show a body of water in front of the glacier, suggesting that it had surged close enough to the coast to eliminate Vitus Lake. Evidence of 20th century surges continues with the 1938 aerial photos of Bradford Washburn, which show a barren area and a terminal moraine marking the extent of a surge which occurred in 1920 according to dendrochronology (Molnia and Post, 1995). Dendrochronology has also been employed to date the 1900 surge moraine, with trees approximately 70 years of age growing in accordance with forest succession from a barren plane following retreat of the glacier (Molnia and Post, 1995).

Washburn's photography in 1938 showed bidirectional crevassing near the Grindle Hills, which represented the beginnings of the 1938-'40 surge (Molnia and Post, 1995). The terminus of Bering Glacier had advanced from 1- 4 *km* by 1940, and had again eliminated Vitus Lake.

Bering Glacier retreated during the period from 1940 to 1959. At the terminus, Vitus Lake attained dimensions of 5 *km* long by 3 *km* wide before the next surge which started in 1959, again closing the lake (Molnia and Post, 1995). Before the 1959 surge, however, many of the smaller ice marginal lakes had become connected. Downcutting of the Seal River mouth lowered the outlet elevation for these lakes which then began to drain into Vitus Lake which discharged via the Seal River (Molnia and Post, 1995). By the early 1950's, the Seal River had captured virtually all of the drainage from the Bering Glacier terminus (Molnia and Post, 1995). This drainage configuration has persisted to the present day.

During the 1957-'60 surge, the terminus of Bering Glacier re-advanced almost 8 *km*, as can be seen in the aerial photographs of Post (1972). This event was followed by a minor surge in 1965-'67, which advanced the terminus 1 *km* further. This second event was treated by Post as a delayed second pulse of the 1957-'60 surge when determining the total offset within the glacier; however, the six year delay may suggest separate events. The two-fold surge advanced the terminus of Bering Glacier to within 1 to 3 *km* of its early 20th century maximum position (Molnia and Post, 1995).

Since 1967 the glacier has been in a state of quiescence and retreat. This trend was interrupted once in 1981 by a short lived "mini-surge" which did not reach the terminus (Molnia and Post, 1995). This event occurred north of the Grindle Hills. The net retreat of the terminus through 1993 was about 12 *km*, which may have represented the most significant retreat of the glacier in recent history. Before 1993 it was publicized that Bering Glacier might be entering a state of irreversible retreat, which could become "catastrophic" (Molnia, 1990; Bush, 1991). It was thought that a new marine fjord system would then develop in the valley of the Bering Glacier if the foreland was eroded away and the glacier became exposed to the Gulf of Alaska (Molnia, 1990; Bush, 1991). Study of the rate of erosion along the coast of the foreland was conducted by the USGS in an attempt to gauge the likelihood of this development. The 1993-'95 surge has reversed the retreat of the glacier, as have all surges during this century, but the overall trend of retreat may not have been reversed.

## Chapter 4: SAR Imaging

### *4.1 Introduction*

The principles of synthetic aperture radar imaging are outlined. SAR is defined, and its advantages and inherent imaging errors are explained. Application to geophysical problems is discussed, with particular emphasis on previous uses of SAR in the study of glaciers and how that has led to this study of the Bering Glacier. Detailed descriptions of the SAR principles summarized here can be found in Curlander and McDonough (1991).

### *4.2 SAR Principles*

Synthetic aperture radar (SAR) is an active microwave sensor that images 100 x 100 km areas of the earth's surface at high resolution. Its ability to interrogate target surfaces regardless of daylight or cloud cover conditions makes SAR an ideal tool for regular observation of study areas. This advantage is particularly important in the mid-to-high latitudes where most of the world's alpine glaciers are located, since these areas are frequently obscured by clouds and winter darkness. This is the basic advantage that made SAR a useful tool for studying the 16 month surge of the Bering Glacier.

In contrast to passive satellite sensors, such as LANDSAT, which collect microwave and visible energy that is either reflected or radiated from the earth's surface, SAR creates its own signal by transmitting energy and measuring the return backscattered from the earth's surface to the satellite antenna. SAR thus provides its own illumination, which allows it to operate regardless of time or weather in the target area. Radar depends

on four basic conditions which are: 1) the ability of an antenna to emit an electromagnetic pulse in a particular direction; 2) the ability to detect, with directional precision, the attenuated signal backscattered from the target area; 3) the ability to measure the time delay between transmission and reception, which gives the range to the target; and 4) the ability to scan with the directional beam and examine a large area (Olmsted, 1993). SAR differs from conventional radars in that the application of spectral analysis to the phase-controlled return signals allows significant enhancement of the four basic principles of radar.

Detection of small Doppler shifts in signals returned to the satellite from targets, between which there is relative motion, allows high imaging resolution, on the order of 3 arc seconds for spaceborne SAR (Olmsted, 1993). The technique depends on precise determination of the position and speed of the satellite with respect to the target, and on integration of the return signal over a time period which is long in comparison with the time between pulses of transmitted energy (Olmsted, 1993).

The techniques mentioned above form the basis of synthetic aperture radar imaging theory. In effect, the algorithms used in SAR processing create a "synthetic aperture" which is needed to obtain a high resolution image from a sensor that is operating at extremely high altitude and is transmitting and receiving microwave energy with wavelengths on the order of 100,000 times greater than that of light. Imaging sensors in general operate by intercepting radiated energy with an aperture of a given physical dimension. In passive systems the angular resolution is controlled by the ratio of the electromagnetic radiation wavelength and the aperture size. The spatial resolution of

the image is the angular resolution multiplied by the sensor's altitude. As the altitude of the sensor increases, the spatial resolution decreases unless the size of the aperture is enlarged. With sensors that collect light and infrared radiation it is possible to obtain a relatively high resolution image from high altitudes with an aperture of reasonable size. With radar, however, the wavelength of the EM radiation is much bigger and the necessary antenna size becomes impossibly large for high resolution imaging. This physical limitation is overcome with signal processing steps which create a "synthetic aperture". For the European Space Agency (ESA) SAR First European Remote Sensing satellite (ERS-1), with an altitude of 785 *m* and an antenna length of 10 *m*, the SAR spatial resolution is 25 *m*, but the real aperture spatial resolution of the antenna would be closer to 20 *km*. To achieve a real aperture resolution of 25 *m*, the SAR antenna would need to be over 8 *km* in length (Curlander and McDonough, 1991). The extreme antenna length that is needed for high spatial resolution is, instead, synthesized in the digital signal processing. This is done by compensating for the phase differences in signals returned from different points within the target area.

For ERS-1, the four conditions of imaging radar are met because the satellite: 1) emits high energy pulses (lasting 37.1  $\mu\text{s}$  at C-band frequency, 5.3 GHz, with a wavelength of 5.66 cm, VV polarization, and peak power of 4.8 kW); 2) receives the low power return signal from the earth's surface; 3) measures the time delay between transmission and reception, thereby recording range to the target; and 4) scans the target because the satellite is moving across the area, and because the direction of the pulse, or

the "look angle", is inclined  $23^{\circ}$  from nadir (vertical) giving all scatters within the target area a unique range in the cross track direction.

The fourth condition, scanning to cover the area, is actually met in two ways. Scan in the along track, or azimuth, direction is achieved by the motion of the satellite. Azimuth resolution is obtained by measurement of the Doppler shift within the returned signal. All scatterers within the image area will have slightly different angles with respect to the track of the moving antenna, so at any given time those scatterers will also have different velocities relative to the satellite. This produces a shift in frequency of backscattered signals which distinguishes returns from different points in the along track direction.

Scan in the cross track direction, or range, is achieved during signal processing when the signal is digitized in time, translating the information into range from the satellite. The inclination of the ERS-1 look angle makes it a side looking satellite, as opposed to nadir looking which has a beam extended on both sides of the nadir track directly below the satellite. In a nadir looking configuration a given signal travel time would correspond to return from both sides of the nadir track. Thus, during signal processing, it would not be possible to distinguish between the left and right sides of the image. In the side looking configuration each scatterer within the SAR footprint is characterized by a unique combination of travel time and doppler shifts. The side looking beam configuration of ERS-1 is illustrated in figure 4.1.

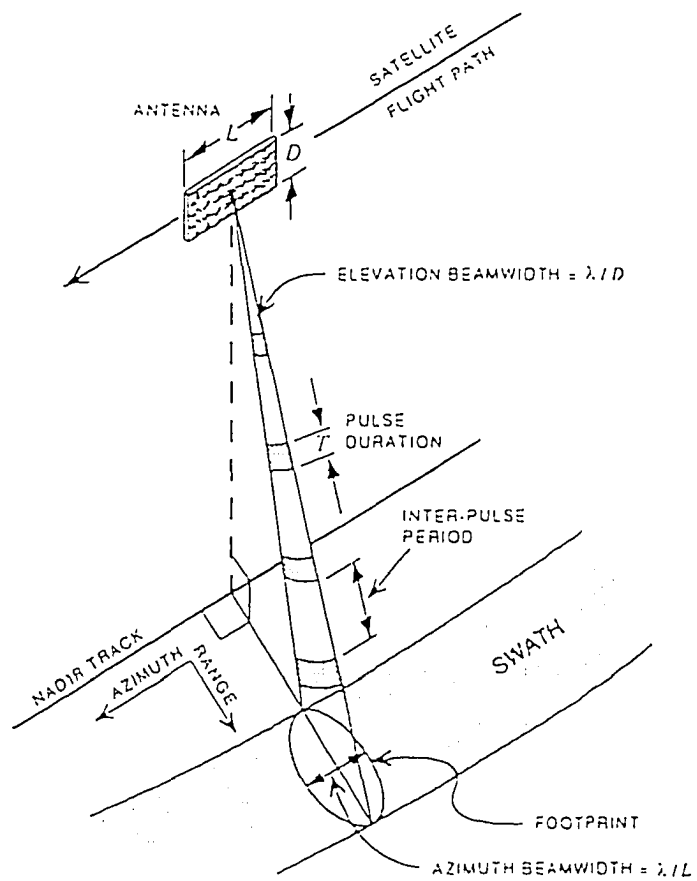


Figure 4.1 Scanning configuration of a side looking SAR satellite, from Olmsted (1993).

### *4.3 Image Errors*

While SAR is useful for repeated observation of surface features, there are a number of geometric image errors inherent to the side looking SAR system which must be addressed before measurements are made with the image data. These errors are related both to the motion and position of the satellite, relative to the target surface, and to variations in terrain height within the target area. Accurate determination of target locations and dimensions depends on the elimination of these errors. This section is intended to motivate the aspects of SAR imaging geometry which must be corrected.

The attenuation of signals returned to the satellite will vary according to the range between the antenna and the target, and the dielectric properties of the surface. The brightness of the backscattered signal will decrease with increasing attenuation and, therefore, with range in an amount proportional to the inverse square of the distance traveled. Range darkening also results from the variation in incidence angle which is  $23^{\circ}$  in the center-range, but is  $21^{\circ}$  in the near-range and  $26^{\circ}$  in the far-range. The result is a general darkening from near to far in the cross track direction. Attenuation will also vary between images of the same target due to variations in the satellite's relative position and heading. These effects are, however, compensated for during the initial SAR processing of ERS-1 data at the Alaska SAR Facility (ASF). Additional errors are related to pixel range and target height variations.

The images from a side or slant looking SAR satellite are presented in a slant-range geometry. Because the signal spreads in a spherical pattern from the antenna, arcs along the same azimuth show ground range areas which will project onto a single image

pixel. As seen in figure 4.2, those arcs are intersected with an image plane which shows the location of returns from the target surface. Because the incidence angle varies across the range, intervals of equal ground range will be smaller in the near range than in the far. In the image this results in compression in the near range and expansion in the far range as is illustrated in figure 4.3. This is the primary range error in side looking SAR imagery.

Errors in the azimuth direction result from the changing velocity of the satellite relative to the target. These effects are called the relative skew and relative scale errors. Relative skew is the fractional error between an angle as shown in the SAR image and the actual angle. Relative scale is the fractional error between distance shown in the SAR image and the actual ground distance. These errors are depicted in figure 4.4.

Errors which result from variation in terrain height are the result of an underlying assumption in the image processing of SAR data; that the satellite is traveling at a constant speed over a smooth earth surface. This assumption is necessary in order to determine the satellite's position and speed after the signal data are collected, a critical variable in the processing procedure. The assumption simplifies image creation, but it often leads to terrain related errors because the smooth geoid cannot accurately represent the earth's varying surface topography.

A moderate to large amount of topographic relief in an image area will result in significant height error. This becomes a cross track position error when projected onto a slant range image, creating an absolute location error which misrepresents a feature's actual position in a geographic coordinate system. This error precludes analysis of terrain

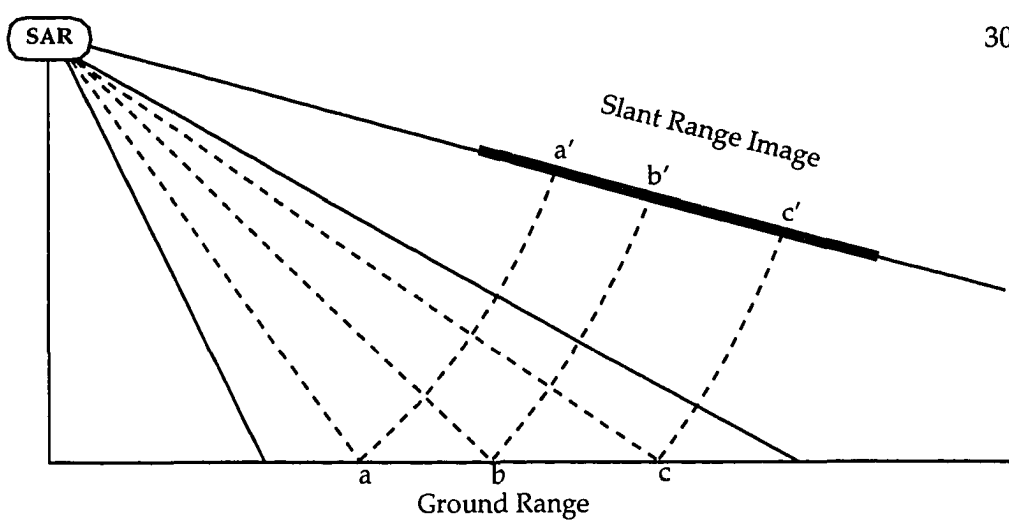
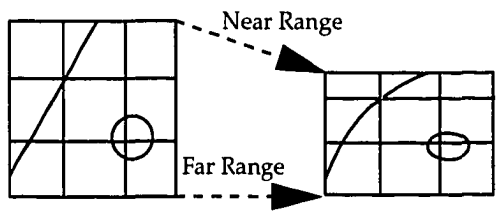


Figure 4.2 The slant range image projection.



4.3 SAR image range distortion.

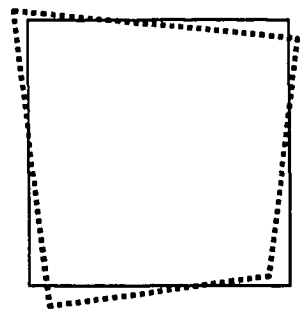


Figure 4.4 Relative scale and skew errors. The square is real image area, the irregular shape shows the actual placement of signals.

features because of the inaccurate pixel placement and must be corrected before image analysis can be done. The terrain correction procedure which compensates for absolute location error will be discussed in Chapter 5. This type of error is depicted in figure 4.5. Also, the height error, and thus the absolute location error, becomes larger with a smaller look angle of the SAR beam. For ERS-1, one meter of height estimation error in the near range equals up to 3 meters of cross track displacement error (Logan, 1994).

Mountainous regions, such as those in Alaska, produce extreme examples of such distortions which can take three distinct forms and depend on the amount and relative orientation of the topographic relief. As illustrated in figure 4.6, the effect of foreshortening can occur when the slope facing the satellite ( $\alpha$ ) is less than the incidence angle ( $\eta$ ) of the SAR beam,  $\alpha < \eta$ . The foreslope of the mountain is compressed in the slant range image while the backslope is stretched. This produces the "leaning" peaks which are characteristic of side looking SAR images from mountainous areas. If the foreslope is steeper than the incidence angle,  $\alpha > \eta$ , the foreslope is mapped onto the pixels of the backslope producing the effect known as layover. This is illustrated in figure 4.7. The third distortion, known as shadowing, occurs when the backslope is steep enough that it cannot be intersected by the SAR beam and is not imaged. The corresponding area in the slant range image contains no data. Shadowing is illustrated in figure 4.8.

Most of the errors discussed in this section must be corrected before the SAR image data are suitable for analysis of surface conditions (based on pixel brightness) and analysis of terrain in a geographic frame of reference. Radiometric calibration and

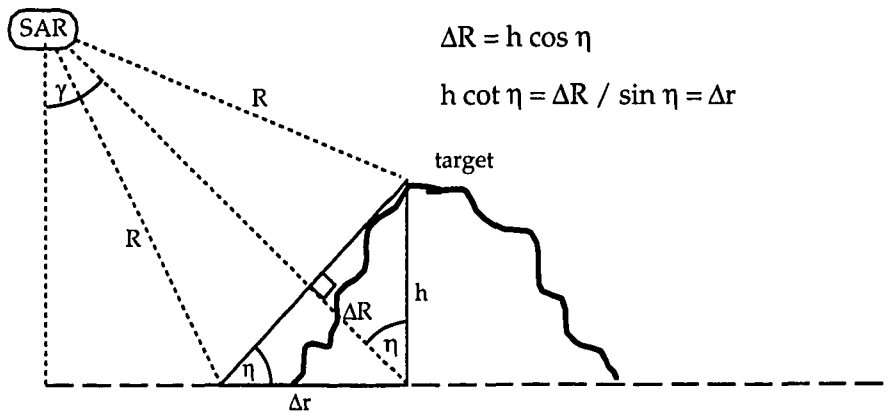


Figure 4.5 Image errors resulting from terrain changes. Height Error,  $h \rightarrow$  Slant Range Error,  $\Delta R \rightarrow$  Location Error,  $\Delta r$ . It is assumed that  $\gamma = \eta$  for a flat earth, and that  $R \gg \Delta R$ .

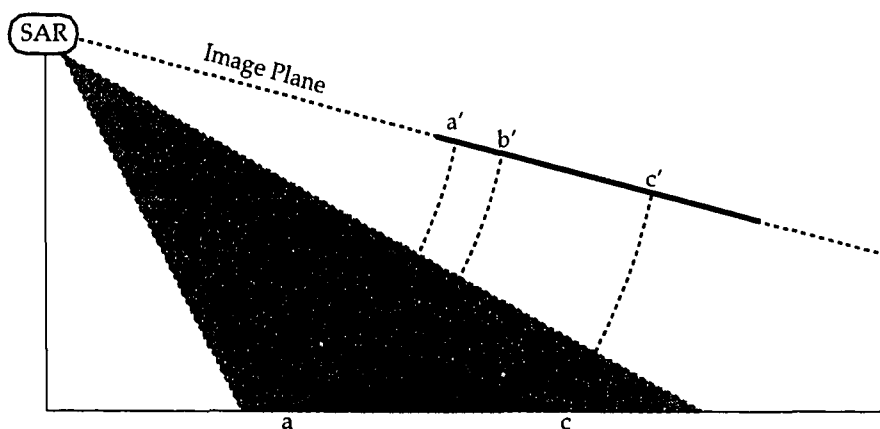


Figure 4.6 SAR image foreshortening.

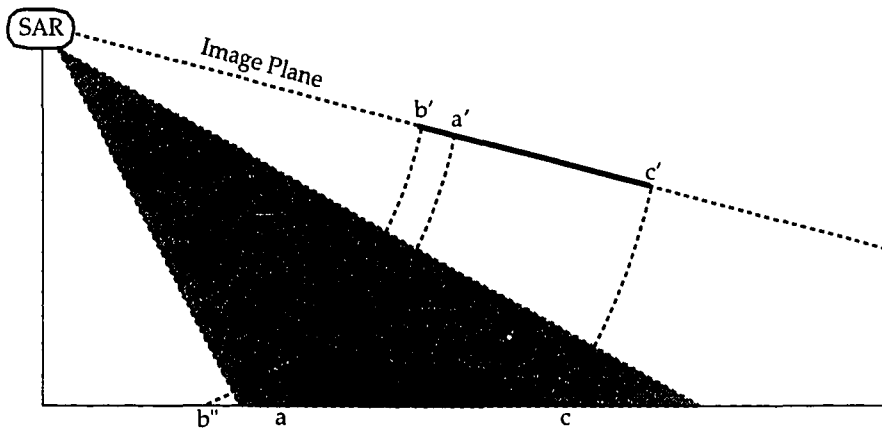


Figure 4.7 SAR image layover.

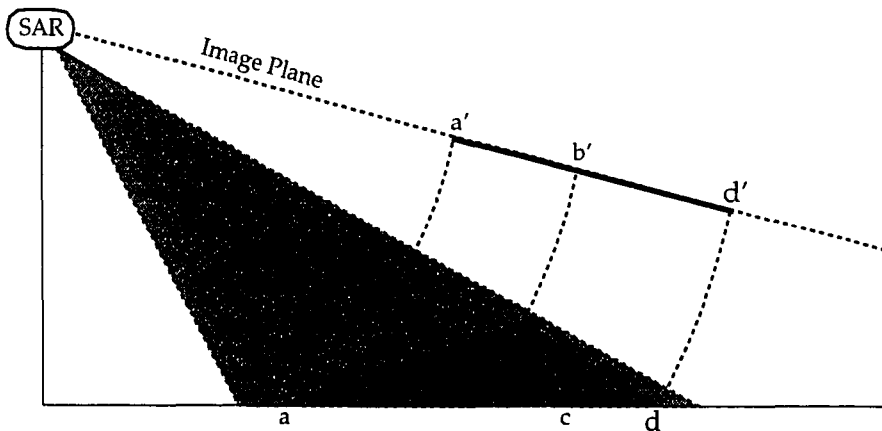


Figure 4.8 SAR image shadowing.

geometric rectification will be the focus of the following chapter, which will detail the methods used to carry out the corrections and to produce an image which can be used to study the motion and surface characteristics of the Bering Glacier during the 1993-'94 phase of its recent surge.

#### ***4.4 Applications***

Synthetic aperture radar is used as a remote sensing tool in numerous earth science fields. Its versatility and regular repeat coverage of most of the earth's surface makes it useful to scientists studying subjects which vary from agricultural production to sea ice motion. This section is intended to provide a brief overview of the general applications of SAR imaging, and to provide a more detailed summary of how SAR has previously been applied to the study of glaciers.

The applications of SAR can be broken down into three basic categories involving surface scattering, volume scattering, and change detection. Surface scattering is defined as the interaction of the electromagnetic wave and the boundary between two dissimilar media (Curlander and McDonough, 1991). The most common interface involved in surface scattering is between the atmosphere and the ground (including soil, rock, ice, or snow) but can also be between air and open water, lake ice, or sea ice, or between ice and unfrozen water. Volume scattering occurs when EM waves intersect particles or spaces within a non-homogeneous material (Curlander and McDonough, 1991). For example, volume scattering can occur when SAR penetrates snow or ice and reflects off ice lenses, water pockets, or air spaces. Both the effects of surface and volume scattering can be

used to classify a target area based on the unique scattering properties of different materials. The total energy backscattered to the satellite is a combination of surface and volume scattering, so an understanding of how EM waves scatter from various media is useful for interpretation of SAR images.

The third category of SAR applications, change detection, has been the basic method used for study of the Bering Glacier surge. Change detection involves the comparison of different SAR images of the same area to see how dynamic features have evolved during the time between the images. The technique has been applied most often to tracking sea ice motion. In the case of Bering Glacier it has been used to detect the onset of the 1993-'94 phase of the surge, and to observe and measure its progression. In general, change detection requires that images be geocoded (reoriented to match a geographic coordinate system) and coregistered before change detection can be carried out. The methods used to geocode and coregister images of the Bering Glacier are discussed in Chapter 5, "Processing". Chapter 6 describes the results of the change detection analysis are presented in Chapter 7, "Results."

Study of glaciers with SAR has not been wide-spread and the bulk of the research has focused on surface and volume scattering from bare ice and snow. The earliest study of glaciers with SAR used imagery acquired by Seasat during mid-summer to early autumn 1978. In a study published in 1983 by Hall and Ormsby, SAR images of the Mt. McKinley and Malaspina Glacier areas of Alaska were coregistered with LANDSAT passive satellite images and used to evaluate the hydrology of those regions. Their results included mention of glacier features which had not previously been observed with

satellite SAR imagery. These included crevassing, moraines, and medial moraines folded and deformed during past surges, and the positions of glacier termini.

Most of the research involving glaciers and SAR in the following years focused on the scattering properties of snow and ice. It was recognized that SAR is uniquely useful because of its ability to penetrate the darkness and cloud cover which frequently obscure glacierized regions (Rott and Matzler, 1987). In the same study it was shown that multi-frequency SARs are useful for glacier study because some differing conditions of snow and ice will respond better to certain wavelengths of EM radiation. Also, this study recognized the important role of snow cover and its seasonal variations in SAR classification of glaciers. The depth and condition of snow was seen to either obscure or reveal the ice surface below. Wet snow causes specular reflection of the SAR beam, returning very little energy to the SAR antenna and resulting in a dark image. Dry surface snow, however, is virtually transparent to SAR and allows the underlying ice to be seen.

SAR has been employed for study of the Greenland ice sheet. Bindshadler and others (1987) used SEASAT and airborne SAR to catalog many features of the ice sheet. They were able to observe crevasses and lineations which indicated flow directions. They also noted a broad tonal variation which corresponded to the ice sheet's equilibrium line. Their observations were, in general, more detailed than any previous study of glaciers with SAR. Further research on the Greenland ice sheet has shown that it is possible to distinguish the different snow facies on the ice sheet (Jezek and others, 1993). Using C-band SAR it was possible to differentiate areas based on the melt processes occurring at varying altitudes. This result was supported by a concurrent study (Fahnestock and

others, 1993) which went a step further and used change detection in sequential imagery to observe changes in surface snow cover and wetness, mass balance, and ice flow. The locations of boundaries between the snow facies were located to within a few kilometers.

A recent thesis by Adam (1995) employed SAR imagery map to the snow line of Place Glacier, British Columbia. By ortho-rectifying SAR data Adam was able to minimize geometric image distortions and geocode the SAR images which were used to classify the glacier surface and map the position of the snow line.

All of these studies demonstrate the direction of research to the present time, and form a small but solid foundation for the practice of studying glaciers with SAR. In this study, change detection is applied more heavily than in most previous research. The effects of surface and volume scattering from the Bering Glacier are not studied. Instead, the morphologies which are seen in the resulting images are observed through time to track the progression of the surge. It is assumed that seasonal changes in the relative proportions of surface and volume scattering do occur, and that these are the result of changing surface conditions on the glacier.

## **Chapter 5: Image Processing**

### ***5.1 Introduction***

The terrain correction process incorporates several image processing procedures which are used to correct both the radiometric and geometric distortions inherent in raw SAR images. The pixel brightness variations that result from range differences within the imagery, and differences in gain during processing of the raw signal data, are corrected with the preprocessing step of radiometric calibration. The dimensional and terrain related distortions are corrected by geolocation of image pixels in three dimensions in the final stage of the terrain correction algorithm.

#### ***5.1.1 Radiometric Calibration***

Radiometric calibration is the first correction applied to imagery in the terrain correction process, before geometric distortions are addressed. The correction removes pixel brightness errors resulting from signal attenuation and SAR receiver state fluctuations, and from processor gain adjustments during processing of the raw data. The result is that pixels will retain independent values resulting only from scattering conditions in the target area, without artifacts from imaging and image processing.

#### ***5.1.2 Geocoding***

SAR images from ASF are projected along the path of the ERS-1 SAR satellite. The result is the images can be oriented with either north or south "up" depending on

whether the satellite was operating in an ascending or descending orbit. Also, the satellite's flight path does not follow meridians of longitude. The result is that image orientation is a function of latitude. Geocoded images are reoriented to conform to a geographic coordinate system. A by product of geocoding several SAR images of the same area is that the images are automatically coregistered.

### ***5.1.3 Geometric Rectification***

The most significant correction applied to SAR imagery in the terrain correction process is the geometric rectification of pixel warping and location errors related both to terrain height and target range. These errors are corrected by registration of the SAR image to a digital elevation model (DEM) which removes the warping and location errors. The result is an image in which all pixels are equally spaced and are properly located within a geographic coordinate system. This removes the relative skew and scale errors and also corrects the cross track displacements resulting from terrain height variations.

The removal of cross track displacement errors effectively removes the layover and foreshortening effects seen in uncorrected SAR images. Shadowing cannot be corrected because SAR data were not collected from shadowed backslopes when the image was acquired. Shadowed areas will still contain noise, or meaningless pixel values. The final result is an image which appears to have been created from a vertical perspective, rather than the oblique slant range perspective of the original SAR image.

## ***5.2 The Terrain Correction Algorithm***

The geometric correction of SAR images in this study was carried out by implementing a terrain correction algorithm originally developed by Charles Wivell of the U.S. Geological Survey's EROS Data Center. The algorithm uses a SAR image and a DEM of the corresponding area to create a simulated SAR image using the imaging radar model for ERS-1. The simulated SAR image is correlated with the real image and the radiometric values of the real SAR image are located by inverting the mapping from the DEM to the simulated SAR image. This results in a geocoded and terrain corrected SAR image. The entire process contains five distinct phases which are outlined in figure 5.1.

1. SAR Image Preprocessing
  - 1.1 Radiometric Calibration
  - 1.2 Resampling
2. DEM Preprocessing
  - 2.1 Windowing
  - 2.2 Change Projection
  - 2.3 Resampling
3. Simulation of SAR image
4. Correlation of SAR and simulated SAR images
  - 4.1 Despiking
  - 4.2 Image Correlation
  - 4.3 Creation of Mapping
5. Geocoding and Geometric correction of SAR image using the determined mapping

Figure 5.1 Phases of terrain correction (from Logan, 1994).

The first two steps apply necessary preprocessing to the both the input SAR image and the DEM, creating uniform radiometric and dimensional scales which will simplify the remainder of the procedure. The third phase, simulation of the SAR image, uses the

DEM and the SAR ephemeris to simulate a theoretical SAR image. Phase four correlates the real and the simulated SAR images and determines a mapping between the two. The final phase applies that mapping in order to geolocate the pixel values in the real SAR image to corresponding DEM coordinates.

### ***5.2.1 Preprocessing***

SAR preprocessing accomplishes two objectives. First, the SAR images are radiometrically calibrated to contain values which are consistent across the range of the image, and consistent with other images. The latter is particularly important for change detection analysis using the final products. Second, the images are filtered and resampled to correspond to the pixel dimension of the DEM being used. In this study a USGS 1 degree DEM was used, with a pixel size of approximately 90 *m*, which was interpolated onto an orthogonal UTM grid with pixels which are exactly 90 *m*.

Radiometric calibration of SAR images removes residual noise, adjusts for processor gain, and converts the backscattered values from a linear to a logarithmic scale (Bicknell, 1992). When the image is created, most of the errors related to the sensor state are removed. However, some residual error remains which must be removed before images can be compared. Cross track residuals are removed by subtraction of a range dependent noise factor. Errors between scenes are corrected by truncation of the backscatter intensity,  $\sigma^0$ , to a standard range (which is specified). In this study, a standard range of  $\sigma^0 = -25.5$  to 0.0 db was used. The linear to log scale adjustment converts values representing pixel brightness to values representing backscatter intensity;

that is, from  $dn$  values between 0 and 256 within the image, to pixel values of  $\sigma^0$ , which represent backscatter intensity. The radiometric calibration process removes artifacts exclusive of those caused by terrain distortion and slopes, giving backscatter values that are calibrated independent of processor gain and are thus comparable among different scenes of the same area.

In order for the SAR image to be registered to the DEM, both must have the same pixel dimensions. Full resolution ERS-1 SAR images have a pixel size of 12.5  $m$ . In this study, the DEM used was a 1-degree DEM (USGS, 1990) interpolated first to a 90  $m$  pixel size in a UTM projection (see section 5.2.2), then interpolated again to a 30  $m$  pixel size. Therefore, the SAR images were resampled from the original 12.5  $m$  pixels down to 30  $m$  pixels using a 3 kernel filter method. To compensate for the increased area covered by each pixel, the average filter kernel is applied to the image first. Because terrain correction is carried out at a resolution of 30  $m$ , the kernel size is 3 x 3 pixels, which is approximately the number of 12.5 meter pixels needed to cover the 30 x 30  $m$  area.

Radiometric calibration and resampling produce a SAR image at a resolution identical to that of the interpolated DEM.

### ***5.2.2 DEM Preprocessing***

A digital elevation model of the SAR image area is needed in the terrain correction process. DEMs are image files in which each pixel represents a geographic coordinate in two dimensions, and an elevation in the third. Visually, increasing elevations are represented as brighter pixel values with zero meters, or sea level, having a

pixel brightness value of zero and increasing pixel values ranging through a grey scale to a maximum value of 256. The DEM employed for this study, the "1 degree" DEM of Alaska (USGS, 1990), has elevation values defined on a 3 arc-second of latitude by 6 arc-second of longitude grid. At the latitude of Bering Glacier, this is approximately 90 x 90 meters.

The first processing step is the windowing of the DEM to correspond exactly to the area covered in the input SAR image. This is done using the metadata which accompanies the SAR image file to find the correct SAR area within the larger DEM. The DEM is then truncated to correspond to the area of the SAR.

The map projection used when terrain correcting SAR images in this study is the Universal Transverse Mercator projection (UTM). UTM is used because the projection unit, meters, is easily transformed to and from image coordinates. The DEM is, therefore, remapped to a UTM projection by interpolating onto an orthogonal grid with 90 *m* spacing. UTM is based on the displacement in meters of a point from the central meridian of the UTM zone that includes that point. Only the UTM coordinates of an image corner point and the image pixel size are needed to map the DEM into the UTM projection.

In order to equalize the dimensions of the DEM and the SAR image, without severely compromising the resolution of the original SAR image, an intermediate pixel size of 30 *m* was selected for the images in this study. The DEM must be interpolated from its original pixel size of approximately 90 *m* to an orthogonal grid of exactly 90 *m* pixels. The final DEM with a pixel size of 30 *m* is then created from the 90 *m* DEM

using a bilinear interpolation method. Conversely the 12.5 *m* pixels of the full resolution SAR image are resampled to 30 *m*.

The final result of the DEM preprocessing steps is a DEM which corresponds precisely to the geographic area and orientation of the SAR image, and which has pixels of equal dimensions. Matching of the DEM to the SAR image allows simulation of the SAR image (i.e., the computation of a synthetic SAR image) at the same scale, and also allows mapping of the SAR pixel values onto the DEM in the final phase of terrain correction.

### *5.2.3 Simulation of the SAR Image*

Phase three of the terrain correction process is the computation of a synthetic SAR image, using the DEM combined with the known position of the satellite at the time of image acquisition. This is necessary in order to establish a mapping between the real SAR image and the DEM. The simulated SAR image, which is based on the DEM, is correlated with the real SAR image in phase four, which permits mapping of the real SAR image onto the DEM.

The simulation of the SAR image is carried out by a module within the terrain correction algorithm called SARSIM. The orbit ephemeris data are used to define the position of the satellite relative to the DEM. SARSIM then generates a synthetic SAR image based on the imaging geometry. The SARSIM procedure contains a SARMODEL which recreates the imaging geometry and the final product is the simulated SAR image needed for correlation with the real SAR image.

#### ***5.2.4 SAR Correlation***

The fourth phase of terrain correction involves smoothing and correlating the real and simulated SAR images, and determining the offset mapping coefficients between them. In order to increase the strength of correlations the two images are first despiked. This is done with a 3 x 3 kernel filter in two passes. The first pass replaces high frequency values with zeros, which removes extreme radiometric variations representing high frequency noise. The second pass replaces points that are far from the mean of the surrounding pixels with the mean value, thus creating smoothed versions of the images.

Next in the correlation phase is the creation of a file of tie-points, which are pairs of image points from the real and simulated SAR (or the search and reference images, respectively) which closely represent the same geographic location. This is done by extracting chips from the search and the reference images. The reference chip is a square of 32 pixels and the search chip is a square of 64 pixels. The smaller search chip is placed within the larger reference chip and a calculation of the degree of cross-correlation is made. The search chip is moved within the reference chip until all possible positions are tried. The one giving the highest degree of cross-correlation is selected as a tie-point. If no position within a given reference chip gives a high enough correlation, the chip is discarded. The entire correlation uses a fixed grid of 1,156 chips (34 columns and 34 rows), of which generally only a subset will yield successful correlations. If sufficient tie-points are not obtained then the correlation fails. Correlation failure occurred frequently when implementing the terrain correction procedure and this was overcome, in most

cases, by decreasing the size of the reference chip, thereby increasing the density and number of possible tie-points.

After a group of tie-points (successfully correlated chips) has been determined, the offset is known for each tie point, where offset means the orthogonal set of displacements needed to match the search chip to the reference chip. Regression methods are then used to attain a least-squares best fit of a low-order polynomial to the offset values for all tie points throughout the image area. The residual error for each tie point is then defined by the magnitude of the difference between the polynomial coordinates and the search image coordinates of the tie-point. If the residual error is too high the tie-point is discarded. The correlation is considered successful if any number of tie-points fit the polynomial coordinates to within 1/2 pixel.

If correlation is successful then the accepted tie-points are used to determine coefficients for a mapping function which gives the offsets between the actual SAR image coordinates and the simulated SAR image coordinates. This is done in both orthogonal directions of the image plane, i.e., in the line and sample directions. The coefficients are then passed to the final phase of the terrain correction algorithm, which results in computation of a corrected SAR image.

### ***5.2.5 Geocoding and Geometric Correction***

The fifth, and final, phase of terrain correction uses the mapping determined in phase four to place the radiometric values of the real SAR image into the appropriate

geographic coordinates of the DEM. This portion of the terrain correction algorithm is called SARGEOM and it creates the final rectified SAR image.

SARGEOM begins by using the mapping (i.e., polynomial) coefficients determined in the correlation phase, and it provides the SARMODEL module with the polynomial coefficients which describe the warping and offsets from the simulated to the real image. SARGEOM calls SARMODEL and the coordinates it receives are the sum of the pixel coordinates of the simulated SAR image (which are functions of the coordinates of the DEM pixels) and the offsets from the simulated to the real SAR image (which are defined by the polynomial). Therefore, the returned coordinates give the pixel in the SAR image that corresponds to a particular pixel in the DEM. SARGEOM uses the returned coordinates to access a pixel value in the real SAR image. That value is then placed, within the final corrected image, at the position of the corresponding DEM coordinates which were given to the SARMODEL.

A particularly concise and useful summary of the SARGEOM mapping process is provided by Logan (1994) and begins with the assumption that  $(x_{DEM}, y_{DEM})$  is the position of a point P within in the DEM, that  $(x_{SIM}, y_{SIM})$  is the position of point P within the simulated SAR image, and that  $(x_{SAR}, y_{SAR})$  is the position of point P within the real SAR image.

"Given

g, the function used by SARMODEL to map DEM points to simulated points,

h, the correlation mapping from the simulated to the real SAR points,

we have,

$$g(x_{\text{DEM}}, y_{\text{DEM}}) = (x_{\text{SIM}}, y_{\text{SIM}})$$

$$h(x_{\text{SIM}}, y_{\text{SIM}}) = (x_{\text{SAR}}, y_{\text{SAR}}).$$

So that,

$$\begin{aligned} (x_{\text{SAR}}, y_{\text{SAR}}) &= h(g(x_{\text{DEM}}, y_{\text{DEM}})) \\ &= (h \bullet g) (x_{\text{DEM}}, y_{\text{DEM}})'' \end{aligned}$$

"The mapping  $(h \bullet g)$  gives the SAR image coordinate which corresponds to the DEM coordinate. The inverse mapping  $(h \bullet g)^{-1}$   $(x_{\text{SAR}}, y_{\text{SAR}}) = (x_{\text{DEM}}, y_{\text{DEM}})$ , is used to place the SAR pixel value from  $(x_{\text{SAR}}, y_{\text{SAR}})$  at the geographic coordinate  $(x_{\text{DEM}}, y_{\text{DEM}})$  in the final corrected image. The inverse function is not actually calculated but the value is taken from the forward function and used in reverse (Logan, 1994)."

The final corrected image has been remapped to correspond to the size and area of the DEM used in the process. Geocoding has been accomplished because the DEM was already mapped in a geographic coordinate system and the SAR image now has the corresponding orientation. Geometric correction is accomplished because the pixels of the real SAR image are now located in their actual geographic locations, removing the cross track displacement errors induced by variations in terrain height. Also, the remapping of the SAR to conform to the area of the DEM eliminates the relative skew and scale errors. The final product, a terrain corrected image, can then be used to locate and analyze terrain features and radiometric signatures within a fixed geographic frame of reference. When the process is repeated with multiple images of the same area, the result

is a set of coregistered images which can be studied in sequence to detect changes in a feature through time. This has been the method applied to sequential imagery of the Bering Glacier during the 1993-'94 phase of its recent surge.

## Chapter 6: Image Analysis

### *6.1 Introduction*

The methods used to measure changing features on the surging Bering Glacier are summarized, and the methods used to create a computer animation of the glacier's motion with sequential SAR images are discussed.

### *6.2 Measurement of Surge Propagation and Terminus Advance Rates*

Both the rate of propagation of the surge front through the Bering Piedmont Glacier and the rate of advance at the terminus of the glacier were measured with sequential SAR imagery. This was possible because the subscenes were coregistered during the terrain correction and geocoding process and each conforms to the same UTM map projection, and has a pixel size equivalent to 30 m of horizontal distance. Each sequential subscene was terrain corrected using the same input corner coordinates which allows the observation and measurement of offsets in glacier features relative to fixed points which include the image corners and fixed objects such as mountain peaks.

The rate of advance of the surge front was determined from four sequential measurements of its mean position between May 19, 1993 and August 25, 1993. This was done by defining a polygon on the images using the routine PUTPOLY in the image analysis software LAS (Land Analysis System). LAS is the primary image analysis tool used in the Alaska SAR Facility's Interactive Image Analysis System (IIAS), a laboratory for scientific image analysis within ASF's Scientific Computing Program. All image

analysis in this study was carried out in LAS on IAS systems which consist of various Sun Microsystems UNIX workstations. The polygon has a fixed baseline in Vitus Lake which is parallel to the east-west UTM axis. The north-south side of the polygons are parallel to the north-south UTM axis and are extended from the baseline to the opposite ends of the surge front. The polygon was closed by defining a line which traces the position of the surge front. The area within the polygon was calculated using the routine MEASURE within LAS. The mean position of the surge front across the horizontal distance of the baseline is the height of a rectangle having a straight line boundary parallel to the baseline, and an area equal to the area of the polygon. The propagation velocity is the change in mean position of the surge front as measured in sequential images, divided by the time difference. This analysis was carried out using four sequential images acquired during the measurement period.

The rate of advance of the Bering Glacier terminus during the surge was measured using the same technique outlined for surge front propagation velocity. In this case the sequence of images that were employed began after the surge front reached the terminus, causing the terminus to begin to advance. The baseline was located along a line in Vitus Lake parallel to the east-west UTM axis and the polygon was defined in the same way. Three successive measurements of terminus advance rate were made and the results are summarized in Chapter 7 ("Results").

### ***6.3 Measurement of Bulge Heights and Estimation of Ice Velocity***

The height of a surface undulation seen in a SAR image can be estimated based on

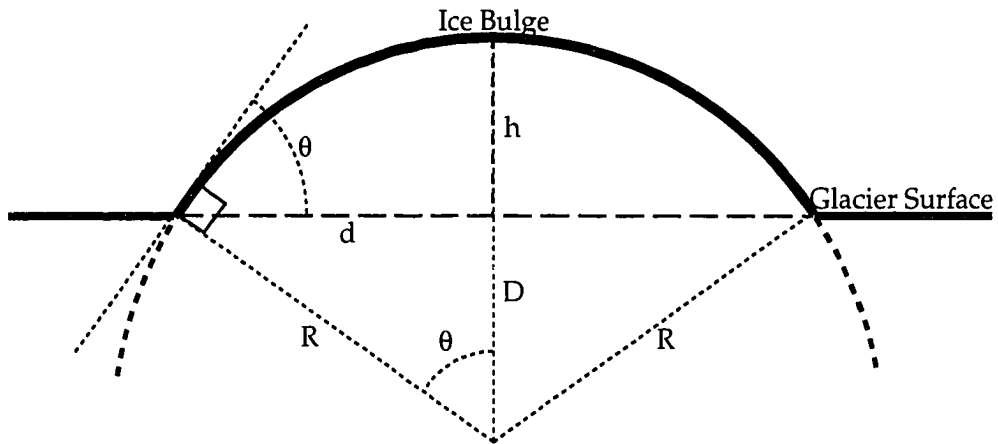
the relative brightness differences which result from the variation in terrain, a method which is similar to the photoclinometry discussed in Bindschadler and Vornberger (1994). This is possible because the brightness of a feature in a SAR image is, in large part, a function of the angle of incidence with the local ground surface. A surface that is inclined towards the SAR will reflect more energy back to the satellite and will have a corresponding increased brightness in the image. This brightness difference can be used to calculate the inclination of the target surface relative to horizontal. The inclination can in turn be used to estimate the height of an undulation if the width of the feature is known. This technique is based on the method of Dr. Shusun Li (of Geophysical Institute, University of Alaska Fairbanks, personal communication) and Binschadler and Vornberger (1994).

The technique was applied to four undulations along the propagating surge front of Bering Glacier before August 25, 1993. These bulges in the ice were seen as roughly circular features on the glacier with bright sides facing the look direction of the ERS-1 satellite, and dark sides facing away. The width of the bulges was measured by calculating the number of 30 m pixels which define a line across the bulge. The average pixel brightness value was determined through random sampling of pixel values on the bright side of the bulge. The same method was then applied to a horizontal ice surface downstream of the advancing surge front. Because the ice surface is smooth and relatively horizontal in the downstream area, the SAR angle of incidence is known to be, approximately, the  $23^{\circ}$  average look angle of the ERS-1 satellite. It is assumed that the other contributors to SAR pixel brightness, surface roughness and dielectric constant,

remain constant over both the undeformed horizontal glacier surface and the undulations, or bulges, upstream in the surge front. Given this assumption, the difference in brightness from the bulge to the flat ice is attributed to the change in surface slope. The brightness difference is referred to as  $\Delta dn$ , where  $dn$  is a measure of image pixel brightness on a gray scale with values from 0 to 256. The  $dn$  value is converted to a value of  $db$  or actual brightness by multiplying by a factor of 0.1 (S Li., personal communication). An initial estimate of the slope angle on the bulge is made and a resultant brightness difference, between a surface with that slope angle and a horizontal surface, is calculated in units of  $db$ . With several iterations it is possible to converge on a theoretical value for the surface slope angle of the bulge which produces a brightness difference equal to that which was measured in the image. This is taken as the actual slope angle on the bright side of the bulge.

Using the half-width of the bulge and the calculated surface slope angle it is possible to estimate the height of the bulge using the trigonometric relationship depicted in figure 6.1. The calculated bulge heights can then be compared to the heights of surge fronts from other known surging glaciers. These results are summarized in Chapter 7. The bulge height can also be used to make an estimate of the actual ice velocity upstream of the bulge using an equation of continuity.

Kamb and others (1985) showed that volume continuity can be used to relate the propagation velocity of a surge front to the ice flow velocity upstream from the front, if the height of the surge front and the ice thickness at that point are known. During the Bering Glacier surge the surge front was defined as the leading edge of the distributed



$$h = R - D \quad \longrightarrow \quad R = \frac{d}{\sin \theta} \quad \& \quad D = \frac{d}{\tan \theta} \quad \longrightarrow \quad h = \frac{d}{\sin \theta} - \frac{d}{\tan \theta}$$

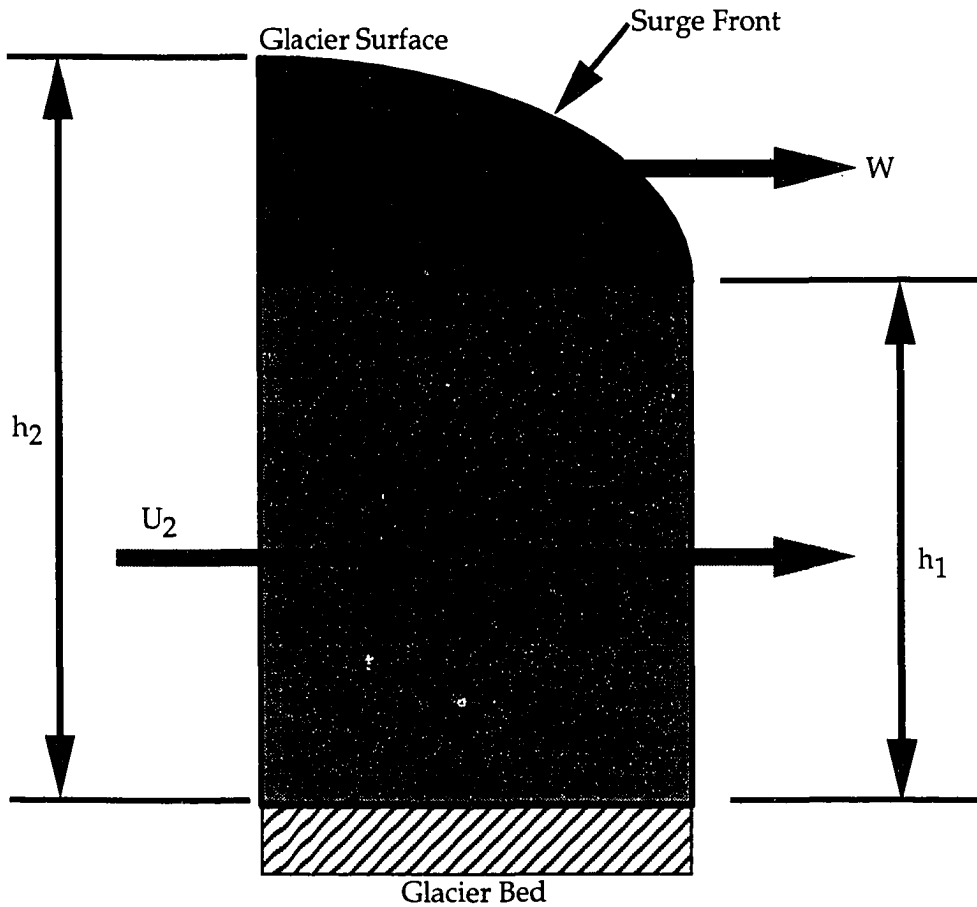
Figure 6.1 Bulge height calculation from SAR derived slope angles is based on the assumption that the surface expression of the bulge is an arc segment of an imaginary circle. The distance from the top of the bulge to the center of the circle is the radius ( $R$ ), and the height of the bulge is that portion of the radius above a line corresponding to the horizontal glacier surface. Using the slope angle ( $\theta$ ) (derived from the SAR image) and half the width of the bulge ( $d$ ), the radius ( $R$ ) and the distance to the center of the circle ( $D$ ) are calculated and the difference gives the height of the bulge ( $h$ ).

region of bulges that propagated down-glacier. The bulge height estimates are, therefore, taken to be point estimates of the surge front height. Rough estimates of the ice thickness were made using USGS radar measurements of the depth of the bed below sea level at discreet locations (Molnia, 1993), combined with the USGS map of the pre-surge ice topography, with a rough adjustment of  $-100\text{ m}$  for downwasting of the ice surface due to ablation prior to surge onset. The resulting rough estimates of ice thickness are used with the bulge height estimates to determine the approximate ice velocities, up-glacier from the propagating surge-front, based on continuity. The equations are summarized in figure 6.2.

The measurements of surge front propagation velocity and terminus advance rate, and the estimates of bulge heights and ice velocities, are used to characterize the surge of Bering Glacier. The results are summarized in the following chapter. Also of importance is the basic technique of observation. The pictorial nature of SAR imagery permits a significant amount of interpretation without actual measurement. A summary of the observed changes on the surface of Bering Glacier follows in Chapter 7.

#### ***6.4 Computer Animation of Sequential Imagery***

The terrain corrected images of Bering Glacier can be viewed in sequence because they have been geocoded and are therefore coregistered. This technique of data visualization is referred to as computer animation; ie., the images are presented in sequence, so that changing features within the images are seen to move relative to the fixed points. The animation of the Bering Glacier surge was created initially by using



$$Q_2 = U_2 h_2 \text{ and } Q_1 = U_1 h_1 \text{ and } Q_2 \gg Q_1$$

SO

$$U_2 = W/h_2 \times (h_2 - h_1)$$

Figure 6.2 Continuity equation for estimation of ice velocity upstream of the propagating surge front.  $Q_1$  and  $Q_2$  are volume fluxes out of and into the cross-sectional area.  $U_1$  and  $U_2$  are, respectively, ice velocities before and after passage of the surge-front. The thickness as a result of the surge wave ( $h_2$ ) is the original ice thickness ( $h_1$ ) plus the height of the bulge measured in SAR imagery.  $W$  is the propagation speed of the surge front as measured in SAR imagery.

11 images covering the period from November 22, 1992 to October 18, 1993. Later versions of the animation have been expanded to include up to 16 images extending through June 1994. All versions of the animation were constructed using Silicon Graphics UNIX workstations, with the assistance of personnel from the Arctic Region Supercomputing Center (ARSC). The original animation, created in December of 1993, was a gray scale series of images without annotation. Successive versions included improvements such as (false) color, and annotation denoting geographic features and time. Final versions of each animation were output to video tape for ease of presentation.

## Chapter 7: Results

### *7.1 Introduction*

The results of the measurements outlined in chapter 6 are presented, and the observations made in the sequential SAR images of the Bering Glacier surge are summarized. Evidence for the apparent time of surge onset is presented. Significant aspects of the computer image animation are summarized. Errors are discussed.

### *7.2 Observations in Sequential Imagery*

Figure 7.1 depicts the lower Bering Glacier on November 22, 1992. North is "up", parallel to the right border. The image is 30.7 km north to south (top to bottom) and is equal in dimension from east to west (right to left). The scenes in figures 7.1 through 7.8 have the same dimensions and depict the same area. The mountains near eastern middle of the image are the Grindle Hills (See Chapter 3, figure 3.1, a Bering Glacier area map). The surface of the glacier on November 22, 1992 is smooth and unbroken. The light bands across the main body of the glacier are medial moraines. The more distinct banding on the western margin of the glacier is the region of folded medial moraines which separates the Bering Glacier from the Steller Glacier tributary of the Bering Glacier piedmont lobe, as described in Post (1972). The sharp contrast break at the bottom of the image is the terminus of Bering Glacier in Vitus Lake. The arcuate bands perpendicular to the terminus are also medial moraines. On the western margin of

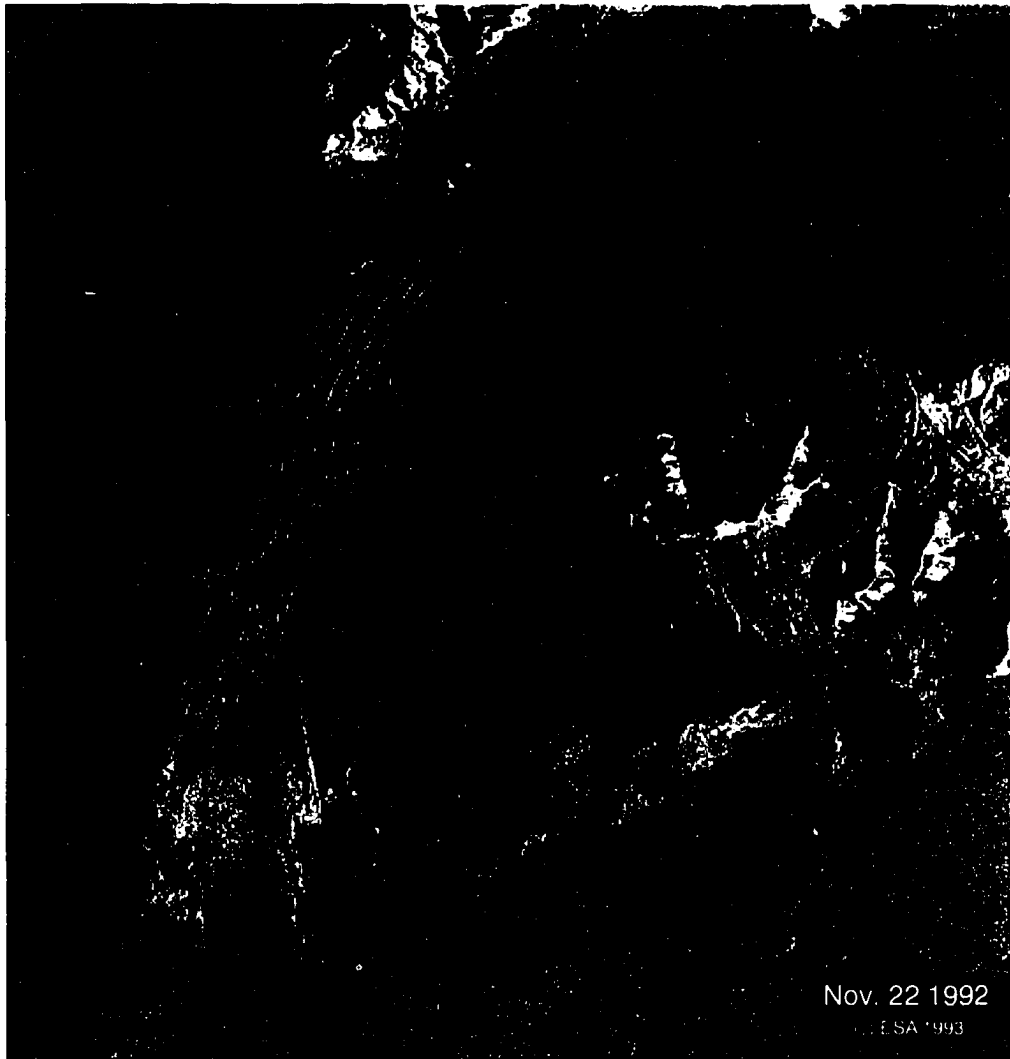


Figure 7.1 SAR image of Bering Glacier on November 22, 1992 showing Bering Glacier in its pre-surge condition. The surface is smooth and unbroken and the terminus is relatively inactive.

the terminus, the deep arcuate embayment is Taslich Arm. Taslich Arm is a fjord like feature which is separated from most of Vitus Lake to the east by the narrow strip of land which emerges perpendicular to the terminus and extends to the southern edge of the image. The striking variations in brightness within Vitus Lake are due to variations in the extent of winter lake ice cover. This image was acquired 4 to 5 months before the onset of surging and shows the glacier in a state of quiescence retreat.

Figure 7.2 shows Bering Glacier on March 26, 1993. This image has not been terrain corrected due to unrecoverable errors in the initial image processing. One benefit of this image is that it illustrates the difference in appearance between terrain corrected and uncorrected SAR images. The image is important because it is the last scene acquired before the apparent onset of surging. The smooth surface depicted in the image shows that the glacier is still largely undisturbed. Vitus Lake is more clearly defined in this scene as it is now mostly free of lake ice cover. The open water acts as a specular reflector and scatters most of the SAR signal away from the satellite, resulting in a low return signal and a dark signature in the image.

The condition of the glacier on April 30, 1993 is depicted in figure 7.3. This image shows surface undulations which have developed in the dark region north of, and adjacent to, the Grindle Hills (arrow 1). A small region of heavy crevassing has appeared directly north of the Grindle Hills near the glacier's margin (arrow 3). This feature, which appears to be a bedrock ridge, has remained constant throughout the period of aerial photography in the later half of this century. An undulation has always been present at this point in the glacier's surface, however, the appearance of large scale crevassing over



Figure 7.2 SAR image of Bering Glacier on March 26, 1993. This is the last SAR image acquired before the apparent onset of surging, showing the glacier is in a quiescent state. Crevassing has not yet appeared on the bulge along the northwestern margin of the glacier (see figure 7.3, arrow 3).

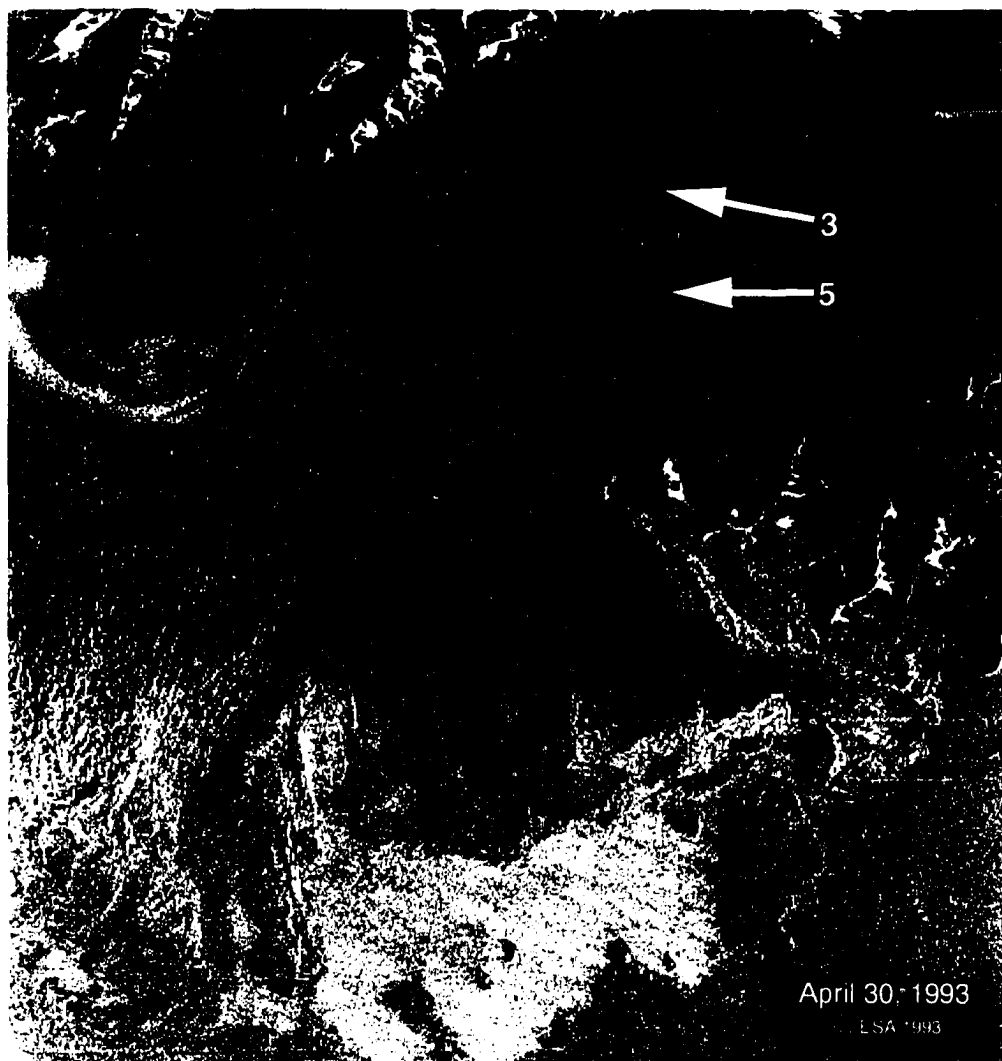


Figure 7.3 SAR image of Bering Glacier on April 30, 1993 showing the first clear evidence of accelerated flow (i.e. crevassing) near the northwestern margin of the valley glacier (arrow 3). Water appears to be ponding between surface undulations (arrow 5). The dark zone above arrow 1 is a region of wet snow on the glacier surface. The transient spring snow line is apparent midway between the terminus and the Grindle Hills (arrow 2). A bright area of crevassing has developed adjacent to the western end of the Grindle Hills (arrow 4).

this bulge in the April 30 image suggests that rapid ice motion has begun. The general transformation of the surface topography appears analogous to the steady-state topography of fast-sliding Antarctic ice streams, which transmit the subglacial bedrock topography efficiently to the surface, causing irregular undulations with local slopes bearing little relationship to the direction of ice flow (Shabtaie and others, 1987; Herzfeld and others, 1993). A small area of crevassing at the Grindle Hills (arrow 4) is a further indication of accelerated flow. It appears, also, that surface water is ponding in troughs between surface undulations (arrow 5).

The dark region on the glacier above the Grindle Hills is the result of water in the surface snow cover. The water saturated snow does not allow the penetration of radar waves, resulting in specular reflection and a dark image signature. The transient spring snow line can be seen midway between the Grindle Hills and the terminus (arrow 2) as it divides a zone of lighter signature at the terminus and an zone of intermediate brightness below the Grindle Hills. This is likely to be the down-glacier limit of a region of discontinuous patchy snow cover. The bright signature of Vitus Lake is probably the result of increased roughness due to capillary waves induced by local surface winds.

Figure 7.4 shows the glacier on June 23, 1993, 2 to 3 months after the apparent time of surge onset. The area bracketed and marked "1", west-southwest of the Grindle Hills, shows a mottled texture which is the region of undulations or surface bulges which correspond to the area fast sliding ice of the advancing surge. The surge front (arrow 2) corresponds to the leading (southern) edge of the area of bulging ice. The dark strip indicated by arrow 3 may be a trough in the glacier which has collected surface



Figure 7.4 SAR image of Bering Glacier on June 23, 1993 in which evidence of surging has become obvious. A region of bulges (bracket 1) is propagating downstream, the dashed line (arrow 2) indicates the surge front. Circles 4a & 4b are surface bulges for which height estimates were made based on SAR image brightness variations. The dark lineation above the Grindle Hills (arrow 3) may be a pond of surface melt water which had collected in a surge-induced trough on the glacier surface.

meltwater. This image is representative of the condition of the glacier when surging activity was first observed at Bering Glacier and, when low altitude aerial photography flights were made on June 19 and 24, 1993 (Lingle and others, 1994). The circled bulges labeled 4a & 4b were used for bulge height and velocity estimates, the results of which are discussed in section 7.4. The tonal variations in Vitus Lake are again due to surface wind activity. The small points of brightness in the lake are icebergs and small islands.

Figure 7.5 shows the glacier on August 9, 1993 about two weeks before the surge front reached the terminus of Bering Glacier. The surge front (arrow 1) has progressed to within about 3.0 to 3.8 km of the terminus. The region of bulging and surface undulation has increased to cover nearly the entire surface of the lower glacier. Fast moving ice has already intersected the terminus in Taslich Arm and significant advancement from the June 23 position is apparent. The arcuate embayment has been replaced by a straight advancing ice margin. Large scale crevassing (arrow 2) has developed up-glacier from the surge front (arrow 1). These crevasses are sub-parallel to the ice flow direction which suggests longitudinal compressive stress as the glacier curves around the bend at the Grindle Hills. The circled bulges marked 3a and 3b will be discussed in section 7.4.

The image acquired on August 25, 1993, figure 7.6, depicts Bering Glacier on or about the time that the surge front intersected the terminus of the glacier (B. Molnia, personal communication). The area of surface bulging has covered the entire glacier with the exception of a narrow strip of smooth ice at the terminus in central Vitus Lake, below the surge front (arrow 2). Rapid terminus advance has already begun in Taslich Arm (arrow 1). Large scale crevassing has expanded (arrows 3). On August 24, 1993 Bering



Figure 7.5 SAR image of Bering Glacier on August 9, 1993. The surge front (arrow 1) has advanced into most of the piedmont lobe. Deformation of the glacier surface is increasing and is evidenced by crevassing (arrow 2) and wide spread undulations and bulges. Circles 3a & 3b are bulges for which height estimates were made based on SAR image brightness variations.



Figure 7.6 SAR image of Bering Glacier on August 25, 1993 corresponding roughly with the time at which the surge front reached the terminus. Advance has already begun in Taslich Arm (arrow 1). Crevassing (arrow 3) has expanded up-glacier from the surge front (arrow 2).

Glacier was observed during a low-altitude flight by K. Echelmeyer and M. Nolan (of Geophysical Institute). The wide spread undulations seen in figure 7.6 are clearly visible in photographs taken by M. Nolan (personal communication). The photos suggest that the undulations may be approximately tens of meters to 100 *m* in height. The surface of the piedmont lobe at this time contrasts strongly with the smooth, nearly stagnant, surface observed in the same region in late June. Also, according to M. Nolan. (personal communication) heavy ice berg calving into Vitus Lake had not begun along most of the terminus, except in Taslich Arm which had been choked with ice bergs before the surge.

By September 13, 1993, the surge front had intersected the entire terminus of Bering Glacier which had begun to advance. As seen in figure 7.7, brightness variations indicate undulations and bulging across the entire surface of the piedmont glacier. The arcuate medial moraines intersecting the terminus have been obliterated. Heavy crevassing has continued to expand (arrows 3). Heavy calving at the terminus has begun and a zone of brash ice bergs can be seen adjacent to the glacier in the western half of Vitus Lake (arrow 1). Advance in Taslich Arm has continued, and deformation of the terminus is apparent. Also, ice can be seen deforming over and around what is probably shallow bedrock immediately up-glacier and to the east of Taslich Arm, adjacent to the area bracketed and labeled "2". This is likely a subglacial extension of the point of land which divides Taslich Arm from Vitus Lake. Arcuate undulations and radial crevassing at the surface appear to be expressions of the stress field induced by flow around this subglacial feature.

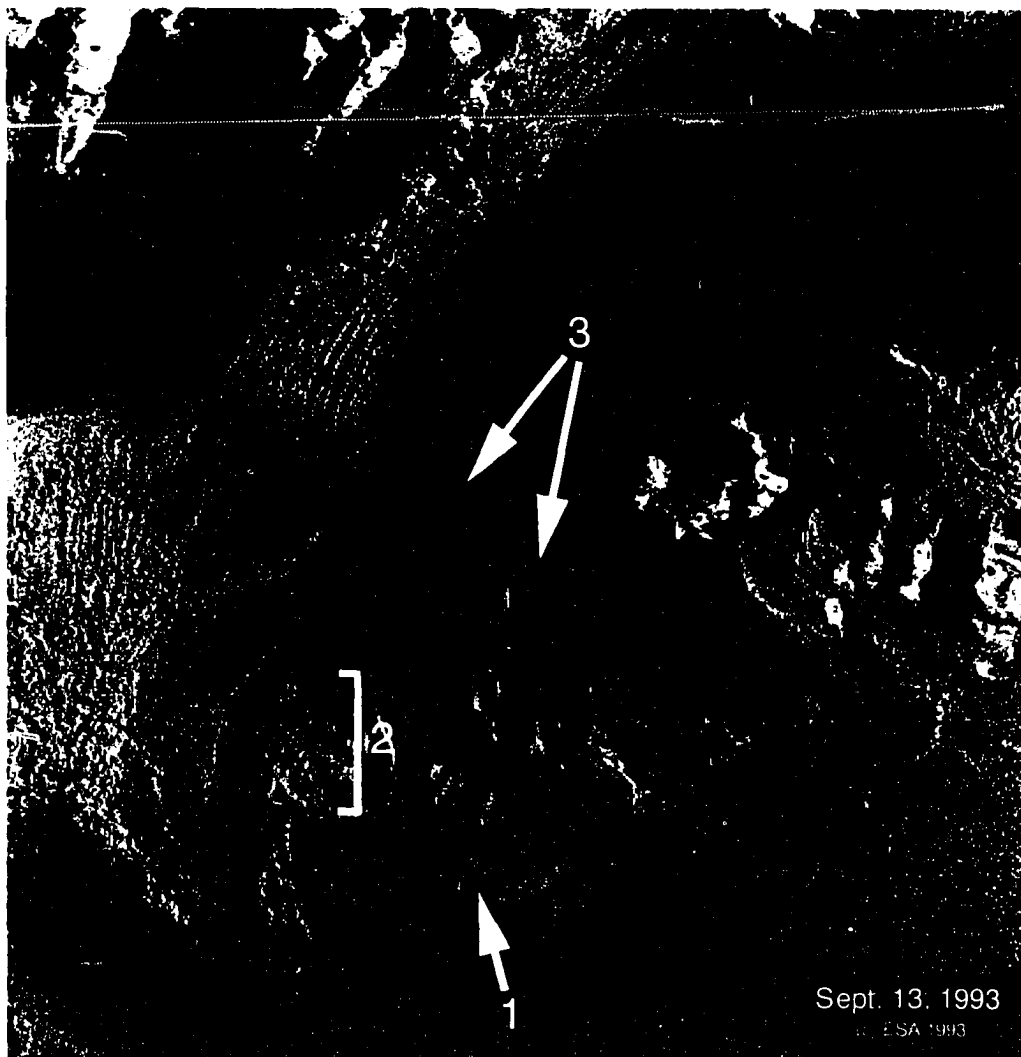


Figure 7.7 SAR image of Bering Glacier on September 13, 1993. Most of the terminus is advancing and calving is evident in Vitus Lake (arrow 1). Crevasse fields have enlarged (arrows 3). Surface deformation is visible around a subglacial high which is probably shallow bedrock (bracket 2).

The final image in the series, figure 7.8, shows Bering Glacier on October 18, 1993. By this time the terminus of the glacier is advancing rapidly across its entire perimeter. Pronounced warping of the medial moraines above Taslich Arm has occurred. The crevasse fields on the glacier's surface have roughly doubled in size (arrows 3). The warping around the subglacial bedrock to the immediate northeast of Taslich Arm is more pronounced (bracket 1). The most significant area of terminus advance is in the central region of Vitus Lake with brackets marked "4". Also, terminus advance has begun over Arrowhead Island (arrow 2) a small point of land on the eastern terminus. Adjacent to Arrowhead Island, the outlet of Tsiu and Tsivat Lakes into Vitus Lake has nearly been cut off. When the closing of that gap did occur later that year, the drainage of the entire eastern margin of Bering Glacier was diverted in to an abandoned river channel further to the east, which flows into Vitus Lake on its southeastern shore.

### ***7.3 Surge Front Propagation and Terminus Advance***

Four sequential positions of the surge front in the central piedmont glacier are illustrated in figure 7.9 and plotted in figure 7.10. This figures represents the irregular polygons used to determine the mean position of the surge front as outlined in chapter 6, section 2. Determining the amount of shortening of the mean distance from the surge front to the baseline from one image to the next, and dividing by the corresponding time interval, allowed the calculation of surge front velocities.

Between May 19, 1993 and June 23, 1993 the surge front advanced 2.62 *km* and the propagation velocity was 75 *m/day*. Between June 23 and August 9, 1993 the surge

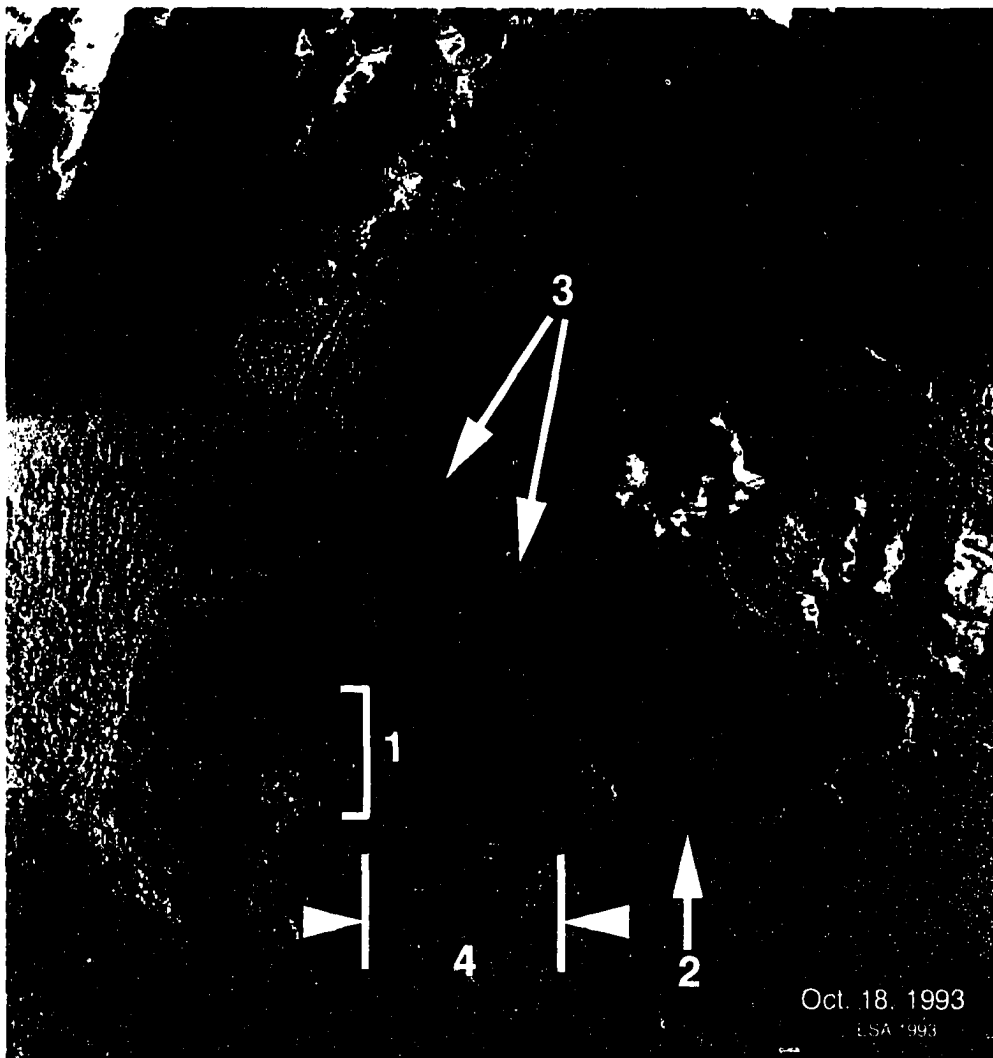


Figure 7.8 SAR image of Bering Glacier on October 18, 1993 showing that the entire terminus is advancing. The most rapid advance is occurring in Vitus Lake (bracket 4). Further development of surface deformations is evident around the subglacial high (bracket 1) and in the expansion of crevassing (arrow 3). The terminus has begun to advance over Arrowhead Island (arrow 2).

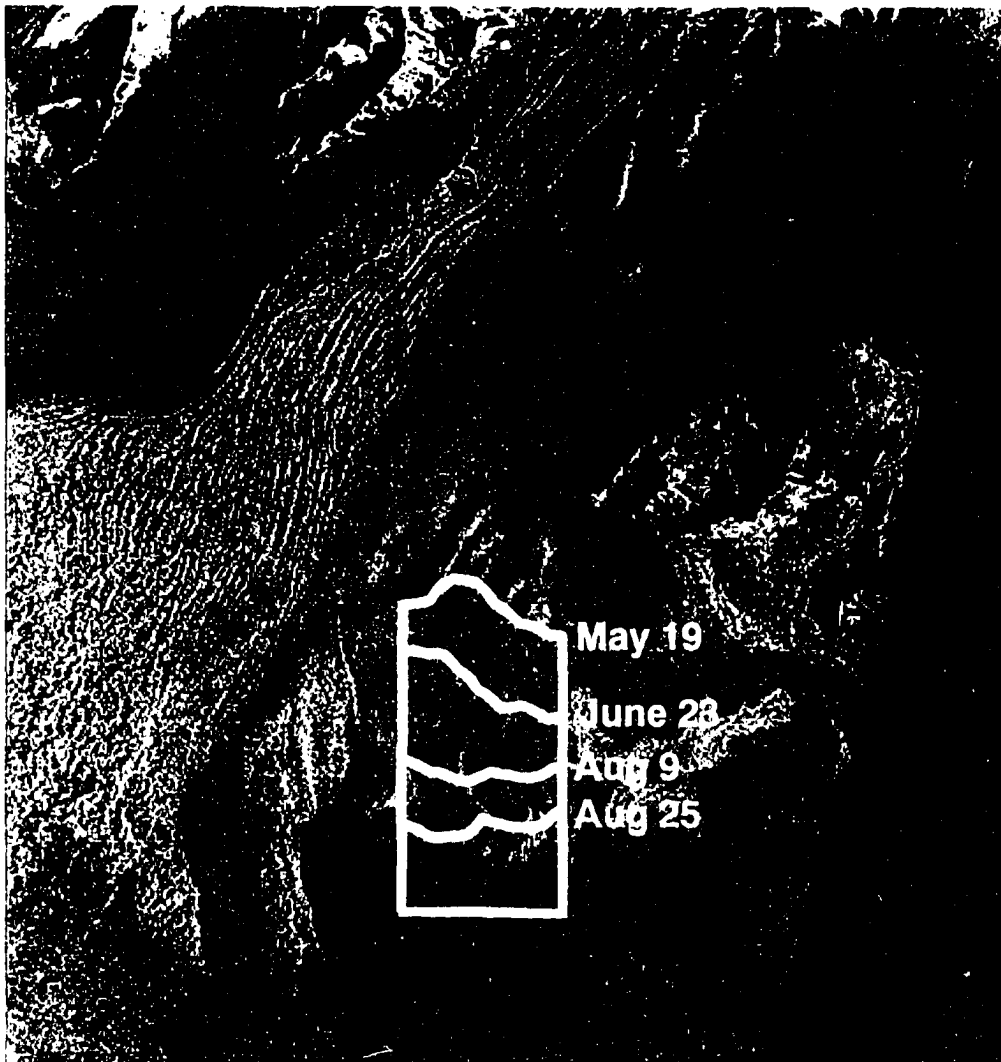


Figure 7.9 Four sequential surge front positions overlaid on a SAR image of Bering Glacier acquired on May 19, 1993 to illustrate how polygons were used to measure the rate of advance of the surge front.

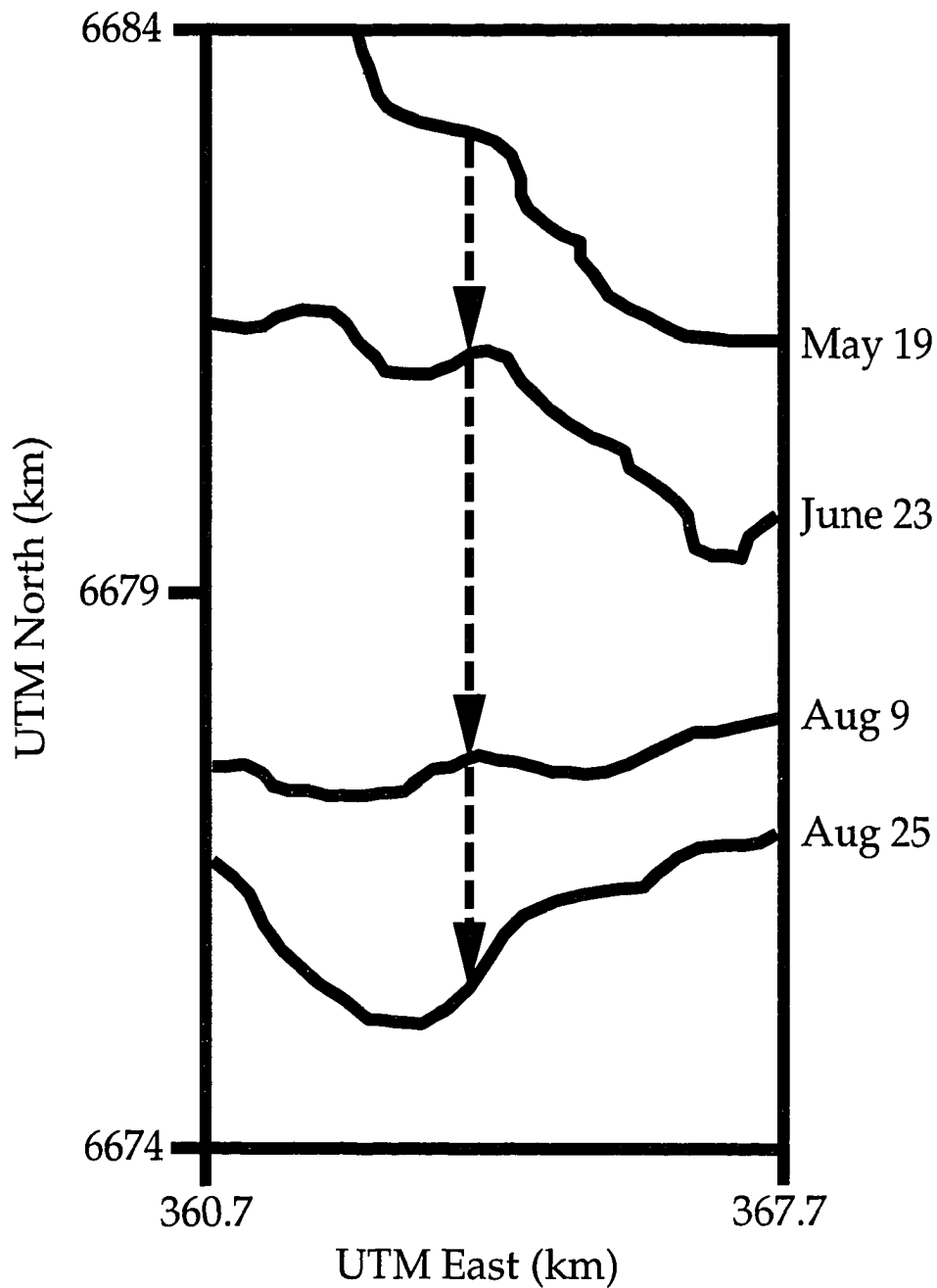


Figure 7.10 Plotted sequential positions of the surge front on the central piedmont lobe of Bering Glacier between May 19 and August 25, 1993, illustrating how measurements of offset were made.

front advanced 4.39 *km* and the mean propagation velocity was 93 *m/day*. There was 1.79 *km* of surge front advance between August 9 and August 25, 1993 corresponding to a propagation velocity of 112 *m/day*. The mean propagation velocity for the entire period, May 19 to August 25, was 90 *m/day*. The accuracy of these measurements will be discussed in section 7.6 (Error Analysis).

The most significant advance at the terminus of Bering Glacier, between August 9 and October 18, 1993, occurred in central Vitus Lake. Measurements of terminus advance were made in this region and are plotted in figure 7.11. The mean position of the terminus and rate of advance were calculated in the same way as the surge front velocities. Between August 9, shortly before the surge front arrived at the terminus, and September 13, 1993, the terminus in Vitus Lake advanced 0.43 *km* at a mean rate of 12 *m/day*. Between September 13 and October 18, 1993, the terminus advanced 0.93 *km* at a mean rate of 27 *m/day*. The mean rate of advance for the terminus in Vitus Lake for the entire period, August 9 to October 18, was 19 *m/day*.

A similar measurement made across the entire width of the terminus of Bering Glacier showed that it advanced at a lesser rate. Between August 9 and September 13 the terminus advanced 0.29 *km* at a mean rate of 8 *m/day*. Between September 13 and October 18 the advance was 0.48 *km* at a rate of 14 *m/day*. Across the entire terminus, the mean rate of advance between August 9 and October 18 was 11 *m/day*.

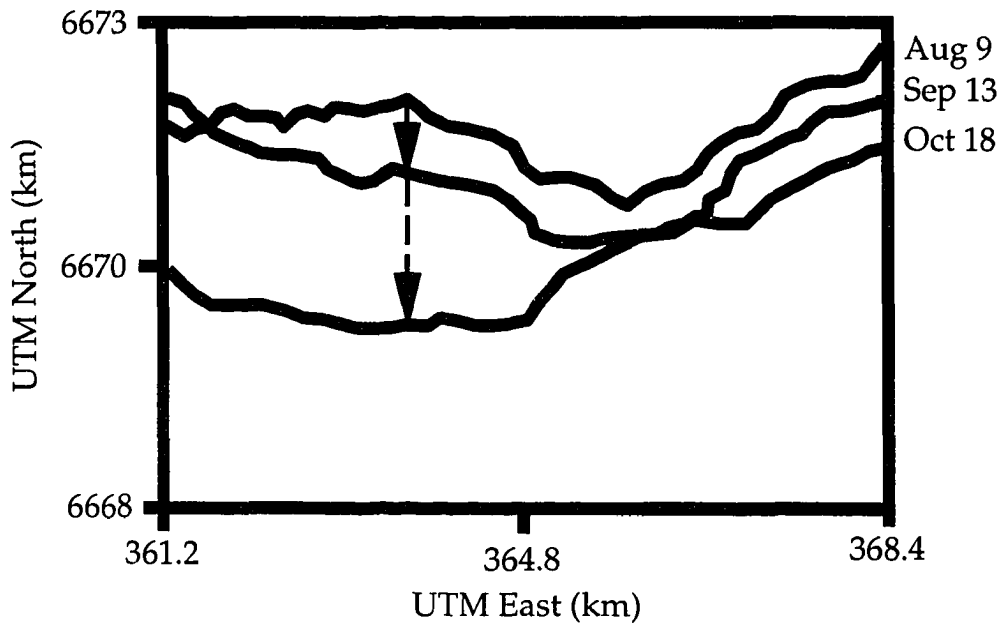


Figure 7.11 Plotted sequential positions of the advancing terminus in central Vitus Lake between August 9, and October 18 1993, illustrating how measurements of terminus motion were made.

#### ***7.4 Bulge Heights and Ice Velocity Estimates***

Applying the methods outlined in chapter 6, section 3, the heights of undulations on the glacier's surface were estimated, and corresponding estimates of ice flow velocity were made for the region immediately up-glacier from the bulges. Bulges 4a and 4b are from the June 2 image (Figure 7.4); bulges 3a and 3b are from the August 9 image (Figure 7.5). The estimated dimensions of the bulges are: (4a) width = 1.6 km, height = 110 m; (4b) width = 1.1 km, height = 70 m; (3a) width = 1 km, height = 60 m; (3b) width = 0.7 km, height = 40 m. These measurements are discussed further, and a comparison to analogous measurements made on other surging glaciers is made, in Chapter 8 (Discussion).

Applying the continuity equation discussed in chapter 6, section 3 (Kamb and others, 1985), the rough estimates of ice flow velocity up-glacier of each bulge are: (4a) 13 m/day; (4b) 9 m/day; (3a) 14 m/day; (3b) 9 m/day. These estimates, which must be considered very approximate, serve to illustrate that the ice flow velocity was likely to have been substantially less than the propagation velocity of the surge front.

#### ***7.5 Description of Computer Animation of Imagery***

The computer animation of sequential SAR images of Bering Glacier is a visualization of the surface motion of the glacier during surge. The final version contains 16 SAR images spanning the time period between November 22, 1992, and June 6, 1994. Surging becomes evident early in the sequence as a diffuse region of light and dark areas which represent the bulging of the surface after (the apparent time of surge onset). This

region then propagates down-glacier, toward the bottom of the frame, radiating into the peidmont lobe until it reaches the terminus in August, 1993. Large-scale crevassing and bulging of the surface are seen to cover the entire glacier, and terminus advance into Vitus Lake then becomes evident. By the end of the sequence the terminus has advanced nearly halfway across Vitus Lake, and is near the bottom of the animation frame.

The SAR animation enables visualization of the surge. The sense of motion is enhanced by the rapidity and smoothness of the image sequence, which conveys motion between images, as well as the changing nature of the surface details.

### ***7.6 Discussion of Errors***

The accuracy of measurements made in terrain corrected SAR images is primarily a function of the image resolution and pixel size. Because the terrain corrected images have a pixel size of 30 *m*, a feature defined by a single pixel in UTM coordinates would have an accuracy of +/- 15 *m*. When considering measurment of the average position of the surge front and terminus, the more significant source of error is the difficulty of repeating measurement of the broad and diffuse boundaries. In order to estimate the uncertainty in the measurement of the surge propagation velocity using the method shown in figures 7.9 and 7.10, the measurement was made twice, starting from the definition of the "polygons." The surge propagation velocities derived from the second measurements were found to agree to within about 14% with the velocities derived from the first measurements. The propagation velocities can thus be taken as accurate to within about +/- 14%.

## **Chapter 8: Discussion**

### ***8.1 Introduction***

The results of this study are placed in the context of other well-studied surging glaciers, and the causes of surging. The Bering Glacier surge is compared to other observed glacier surges, and the light this sheds on the theory of the surge mechanism is discussed.

### ***8.2 Comparison With Other Surges***

The relevance of this study of the Bering Glacier surge depends mainly on a comparison with other surge events. Because the causes and mechanisms of surging are still largely open questions, the importance of each new event which can be studied comes from determining its place within the larger body of knowledge. A number of surge events have been studied during the last three decades and the conclusions are seldom the same, although there are trends which suggest commonalities among surging glaciers. The discussion that follows is modeled largely on a corresponding discussion in Harrison and others (1994), in that the known characteristics of the Bering Glacier surge are compared and contrasted with the conclusions of some of the more important published works on surging glaciers. In particular, the Bering Glacier surge will be compared with the surges of Variegated Glacier (Kamb and others, 1985), Medvezhiy Glacier (Dolgushin and Osipova, 1975), and the West Fork Glacier (Harrison and others, 1994).

### **8.2.1 Size and Setting**

The Bering Glacier-Bagley Icefield system is the world's largest temperate surging glacier. A rough estimate based on the ice velocity and approximate transverse cross-sectional area northwest of the Grindle Hills, suggests that its ice volume flux during surge is comparable to that of fast-flowing ice streams in Greenland and Antarctica (about 15-25  $km^3/yr$ ). It is distinguished from (for instance) Jakobshavns Glacier in Greenland by its periodic (as opposed to continual) fast flow. Jakobshavns Glacier's continual fast flow may be due mostly to internal deformation (Fastook and others, 1995). Ice Stream B in West Antarctica has been shown to flow rapidly via deformation of a porous, water saturated, pressurized layer of subglacial till (Blankenship and others, 1986). It is not known whether this mechanism plays a role in the fast motion of Bering Glacier during surge.

Despite its size, however, Bering Glacier is most comparable to the smaller temperate surging glaciers of Alaska and Central Asia. Bering Glacier is not significantly thicker than most temperate glaciers in Alaska, with ice depths ranging from 300 to 500 meters (Molnia, 1993; Grecn [unpublished], 1993; Molnia and Post, 1995) Like the Variegated Glacier, Bering is situated in coastal Alaska in a area of high precipitation. West Fork Glacier in the central Alaska Range and Medvezhiy Glacier in the Pamirs of Asia are located in continental climates and receive considerably less precipitation. All four glaciers, however, probably have temperate beds. Bering Glacier surges with a recurrence period of 25-30 years which is slightly greater than that of Variegated Glacier, and is 20 to 25 years less than that of West Fork Glacier. It is likely that the similar

recurrence interval for Bering and Variegated Glaciers is due to the fact that they are both located in a maritime climate and should receive similar amounts of annual accumulation. This would allow them a roughly equal period in which to reach a thickness profile which may be critical for surging, as suggested by Raymond (1987). The longer period for West Fork Glacier is probably due to the relatively lower rate of accumulation in its dryer Alaska Range location.

Bering Glacier, like West Fork and Variegated glaciers, lies in a complex tectonic environment. The valleys which all three glaciers occupy are on, or are near, major faults and tectonic boundaries. This suggests that their beds may be composed of easily erodable materials which could result in deformable basal sediments and complicated water drainage systems (Harrison and others, 1994). Harrison and others (1994) suggested that such complex bed conditions may be one necessary factor for a surging glacier. There are numerous non-surging glaciers in these areas, such as the Steller Glacier adjacent to Bering Glacier, which suggests that additional conditions are also required for surging.

### ***8.2.2 Time of Surge Onset***

Observations of the sequential SAR images indicate that accelerated motion was in progress, within the imaged area, between March 26 and April 30, 1993. The development of previously unseen bulging and crevassing in the April 30 SAR image (figure 7.3) indicates that rapid flow had begun as the glacier exhibited deformation in the area of the "Khitrov Hills Bulge" (figure 7.3, arrow 3). This time of onset is consistent

with the observation that most surges initiate during winter (Raymond, 1987). Not all surges have begun in winter, however, and the timing of a winter initiation can vary.

The surge of Variegated Glacier occurred in two phases, the first beginning in January 1982, and the second in October 1983 (Kamb and others, 1985). Like the West Fork Glacier surge in 1987-88, the two phases of the Variegated surge terminated in late June and early July, respectively. The West Fork surge, however, initiated in August, and stands as an exception to the trend of winter initiation. This raises questions about the causes of rapid motion. Raymond (1987) discussed a theory of surge initiation which involves the late season shutdown of the water supply for a temperate surging glacier. As ablation and melting slow to a halt, the amount of water in internal passageways decreases and can no longer balance the inward flow the ice. The water within the glacier might then spread out into a linked cavity network at the bed which would saturate basal sediments and cause the failure of a deformable bed, or cause rapid basal sliding on a hard bed. This model implies that surging would initiate at or before the minimum water input in mid-winter. The January initiation of the Variegated surge may conform to this idea, as well as the surge of West Fork if the water input became low enough at the end of the melt season in August for passageways to contract and collapse. The time of onset at Bering Glacier, however, seems not to be in accordance with this view because its surge initiated well after the probable mid-winter minimum water input, and well before the late-summer end of the melt season. It is possible that water input from early season melting may have played a role in the onset of surging. However, because the Bering Glacier surge seems to have begun at an unexpected time of year, water input and the

effectiveness of water drainage passageways may not be the only factors which control the time of initiation.

Bering Glacier also surged in two pulses, the first phase being the primary concern of this study. That phase lasted approximately 15 months and terminated in late July of 1994. The second phase may have again begun in late-winter or early-spring 1995 and terminated in August 1995 according to the observations of pilot S. Raney (personal communication). The time of surge termination does not show as significant a trend among glaciers as does the time of initiation (Raymond, 1987). While it may be common for surges to terminate early in the melt season when abundant water can reopen the internal drainage system, as seen for Variegated and West Fork glaciers, that is not always the case as shown by Peters Glacier, which ended its recent surge in winter (Echelmeyer and others, 1987). It has been observed that after a surge front has reached, and caused the advance of, a glacier's terminus, the surge can terminate at any time (Harrison and others, 1994). This point is important for Bering Glacier which terminated both phases its recent surge near the end of the melt season when water input was probably low and could not have reopened a collapsed conduit system.

### ***8.2.3 Surge Propagation, Ice Velocity, and Terminus Advance***

The Bering Glacier's flow characteristics were not studied in detail during the surge and the measurements in this study represent some of the only available data, in addition to time lapse photography by the USGS, and a few spot measurements of terminus advance rate and ice velocity made by the author (of Geophysical Institute,

University of Alaska Fairbanks) and K. Lohuis (of Albion College). Terminus advance rates on land along the eastern margin of the glacier were measured in June and July of 1994 and peaked at  $2\text{ m/day}$ , decreasing to  $0.5$  to  $0\text{ m/day}$  by the end of the first phase of the surge in late July. It should be noted that terminus advance on land was seen to be much less significant than in the adjacent deep basins of Vitus Lake. This is probably because the ice flow was greatly impeded where the glacier had to come up from a deep bed to advance over topographic high points. Ice velocities measured by Roush and Lohuis, using differential GPS surveying of several stations up-glacier from the Grindle Hills, showed ice flow velocities between  $10$  and  $20\text{ m/day}$  in mid July 1994. These values give approximate confirmation of the validity of the ice velocities estimated from bulge heights using continuity relationships in the 1993 SAR imagery.

These limited data on the flow characteristics of Bering Glacier during its surge are roughly consistent with those of other observed surges. The advancing surge front on West Fork Glacier was measured at an average rate of  $78\text{ m/day}$ , and was described as being "reasonably well-defined" (Harrison and others, 1994). Applying the same continuity equations as used in this study, Harrison and others (1994) estimated an ice flow velocity immediately up-glacier from the surge front of  $23\text{ m/day}$ . In phase two of the Variegated surge a surge front propagated down-glacier like a wave with a height of the order of  $100\text{ m}$ , at a nearly constant rate of  $80\text{ m/day}$  (Kamb and others, 1985). Detailed ice flow measurements on Variegated Glacier showed that velocities ranged from  $2$  to  $65\text{ m/day}$ .

The rate of surge front propagation for the Bering Glacier falls within and slightly above the range for West Fork and Variegated glaciers. It is likely that the propagation speed was within the 75 to 112 *m/day* range determined from the sequential SAR imagery. Measurement uncertainty was caused by the diffuse nature of the Bering's surge front, which was in contrast to the well-defined surge fronts of West Fork and Variegated glaciers. That is, measurements of surge front position could not be made across the distributed region of bulges which defined the surge front on Bering Glacier. There is, however, an approximate similarity among the propagation speeds for all three glaciers.

The fact that Bering Glacier's surge front was not a clearly defined wall of ice is important because it is the first time such a morphology has been observed. It seems likely that this is a result of the absence of confining valley walls in the piedmont lobe of the glacier. Both the West Fork and Variegated glaciers exist in relatively narrow, steeply walled valleys while the observed portion of the Bering Glacier surge occurred in the unconfined reaches of the lower glacier. Conclusive evidence of how the surge may have propagated up-glacier into the more confined Bering Glacier and Bagely Icefield has not been found. It would be a logical follow up to this project to review the archive of SAR imagery to determine how the surge propagated up-glacier. Nevertheless, it seems evident that the absence of confining valley walls allowed the surge to expand transverse to the flow direction within the piedmont lobe. This absence of lateral constraint may have contributed to the diffuse nature of the surge front.

The rates of terminus advance for Bering Glacier as measured in the SAR imagery seem to be consistent with the ice velocities which were estimated in the SAR images and

measured further upstream by GPS surveying. The terminus advance rate in Vitus Lake is assumed to be the ice flow velocity less the rate of calving. While the surge front never reached the terminus of either West Fork or Variegated glaciers, the 1963 surge of Medvezhiy Glacier advanced its terminus by as much as 1.5 km (Dolgushin and Osipova, 1975). This was seen to occur at rates as high as 105 m/day over a period of two months.

The Medvezhiy Glacier is also significant because, like Bering Glacier, its surge initiated in the ablation area and propagated both up and down-glacier. In fact, the Medvezhiy Glacier surge was confined to the ablation area as it propagated up-glacier to the base of an icefall then stopped. It is not uncommon for surges which initiate in the ablation area to halt at a break in slope farther upstream. Bering Glacier was probably an exception to this rule because it does not have a significant break in slope over its entire length and evidence of surge related crevassing was reported up to and within the Bagely Icefield (B. Molnia, personal communication; C. Lingle, personal communication).

#### ***8.2.4 Surge Termination and Flooding***

As mentioned in section 8.2.2, the late July time of termination for the 1993-'94 phase of the surge of Bering Glacier may not have been significant. The way in which the surge ended, however, was very significant and is consistent with most theories on the mechanism of surging. On July 27, 1994 a catastrophic outburst flood of sediment laden water from the bed of Bering Glacier occurred along the eastern terminus at Tsivat Lake. This tremendous discharge of water, which had been in progress for at least 10 hours when it was first observed, lasted at least two weeks and carved a canyon in the glacier

extending from its surface to its bed and which extended nearly a kilometer upstream. This event coincided with the end of fast ice motion at Bering Glacier in 1994, as observed by B. Molnia (personal communication).

Surge-ending floods have been observed at Variegated Glacier and West Fork Glacier. Flood waters were laden with sediment, indicating release of water stored at the glacier's bed. By contrast, discharge of water from these glaciers was low to non-existent during their surges, also indicating subglacial storage. It is not known exactly how much water was being discharged during the Bering Glacier surge because so much of the glacier terminates in deep fresh water. The duration and intensity of the surge-ending flood, however, suggest that a large volume of water had been stored at the glacier's bed. This points to the commonly referenced mechanism of basal water storage which may operate in most if not all glacier surges.

Finally, there appears to be a factor peculiar to the Bering Glacier which has caused the surge-ending outburst flood to occur at the same point along the glacier's terminus for both phases of surging in 1993-'94 and 1995, and also for the surge in 1967. The point of discharge in Tsivat Lake on the glacier's eastern margin was the same for both of the recent events as observed by the author (of Geophysical Institute) in 1994, and S. Raney (of Fishing and Flying Inc.) in 1995. Aerial photographs taken by Austin Post after the 1967 surge show a canyon in the glacier, at approximately the same location, similar in size and appearance to that which was created by the 1994 outburst flood (A. Post, of U.S. Geological Survey, personal communication). Although there are no conclusive data which indicate why the surge-ending outburst flood occurs in the same

location for successive surges, the consistency of the flood location must be significant. A possible explanation is that there is some kind of irregularity in the glacier's bed topography, which persists between surge events, that is channeling basal water to one point at the terminus. In fact, if such an irregularity exists in the form a trough which captures basal water drainage in the piedmont lobe of Bering Glacier, one would expect significant drainage to occur at this point during the periods between surges as well. Before the surge a significant outflow of water was observed from Tsivat Lake into Tsiu and Vitus Lakes by the author, but it cannot be determined what percentage of the total discharge this represented because most of the glacier terminates in water.

Preliminary data which supports the case for existence of a subglacial channel has been collected by the U.S. Geological Survey. A series of ice thickness measurements on the peidmont lobe of Bering Glacier indicate that the deepest portion of the lower glacier exists near the eastern side, upstream from the point of the outburst flood (Molnia and Trabant, 1992; Trabant and Molnia, 1991). It is possible that this depression in the bed topography is the main channel for basal water flow under the lower glacier, and that this drainage configuration persists throughout multiple surge and quiesence cycles (D. Trabant, of U.S. Geological Survey, personal communication).

### ***8.3 Surging Activity in 1995***

As noted in the previous section, and in section 8.2.2, surging activity resumed at Bering Glacier in 1995. Although this most recent event was not included in this study, the fact of its occurrence, and the observed timing, are significant. According to S. Raney

(personal communication), advance of the Bering Glacier terminus began again in April of 1995, and was evidenced by buckling and compression of the winter ice on Vitus Lake, which had remained undeformed throughout that winter. The previously undeformed lake ice suggests that the glacier had not been advancing significantly prior to April and that it had remained quiescent throughout the winter following the 1993-'94 surge. Between April and late July, 1995 the glacier advanced its terminus approximately 1 *km*. According to S. Raney, the terminus motion appeared to cease in July. An outburst flood of similar proportions to the 1994 event occurred at the same point on the eastern margin of the glacier in mid-September, and lasted approximately one and a half weeks.

The second pulse of the Bering Glacier surge is consistent with the two-pulse surge observed at Variegated Glacier in 1982-'83. The late winter initiation of both fast ice motion events at Bering Glacier seems correlative, and may be due to annual hydrologic conditions which initiated a transition to increased water storage at the bed, accompanied by elevated subglacial water pressure. The August-September flooding and end of fast ice motion in both 1994 and 1995 further suggests that annual variations in hydrologic conditions are affecting surge activity.

In summary, the two phases of the recent Bering Glacier surge must be considered successive pulses of the same surge event. As of this writing (autumn to mid winter 1995-'96), Bering Glacier is quiescent and no surge-type motion is evident. It is likely that the 1993-'95 surge has ended.

## Chapter 9: Summary and Conclusions

A surge of the Bering Glacier, a 185 *km* long temperate glacier located in southcentral Alaska's Chugach Mountains, became evident in satellite SAR imagery between March 26 and April 30, 1993 and continued until August of 1994. Surge activity resumed in April of 1995 and continued until late in the summer of that year (S. Raney, personal communication). The previous surge had occurred in two pulses from 1957-'60 and 1965-'67 (Post, 1972). All of the glacier below the Bagely Icefield was affected by the recent surge, and it is likely that surge motion propagated up-glacier into the icefield as well, as indicated by the observation of fresh crevassing during the surge (B. Molnia, personal communication). At the beginning of the surge, a surge-front developed adjacent to the Grindle Hills and propagated down-glacier as a distributed region of bulges, ranging from 40 to 110 *m* in height, at a mean rate of 90 *m/day*. Ice flow velocities immediately up-glacier from the propagating surge front were estimated from continuity at 9 to 14 *m/day*. The surge-front reached the terminus in late-August of 1993 and the terminus began to advance at rates of 12 to 27 *m/day* in Vitus Lake, continuing through October 18, 1993. The mean rate of advance over the entire terminus, between late-August and October 18, was 11 *m/day*. The first pulse of surge motion ended in August of 1994 with the cessation of advance at the terminus, according to the observations of B. Molnia (personal communication). This occurred at about the same time as an outburst flood of sediment laden water from the base of the glacier along its

eastern margin. Observations by S. Raney (personal communication) indicate that surge motion resumed in April of 1995 and continued until August. An outburst flood occurred in mid-September of 1995, at the same location as the flood in 1994, 4 to 6 weeks after the apparent end of surge motion in 1995, as indicated by the cessation of terminus advance.

Comparison of the Bering Glacier surge with the surges of West Fork Glacier, Variegated Glacier, and Medvezhiy Glacier shows both similarities and differences in the form and possible mechanisms of each surge. Of these, the Alaskan surging glaciers are located in complex tectonic settings and it is possible that faulted bedrock and debris comprise unstable layers beneath all, which may be an important factor influencing surge activity, as suggested by Harrison and others (1994).

The timing of surge initiation and termination differs for all of the glaciers, most especially for Bering Glacier which began and ended its recent surge at about the mid-points between the times of maximum and minimum meltwater inputs to the glacier, which are assumed to be in January and July respectively. This may be a departure from the idea that surges begin between the time of meltwater decrease and minimum meltwater input, as suggested by Raymond (1987). It is noted that the time of initiation at West Fork Glacier also differed from the idea of Raymond (1987), but it was determined that the late-August initiation was near a time of little or no surface melt for glaciers in the region (Harrison and others, 1994). The April initiations of surging at Bering Glacier occurred after the probable beginning of melting and water input. The late-July/early-August terminations of both pulses occurred nearer to the assumed maximum meltwater

input in mid-summer than to the assumed end of the melt season in late-summer/early-fall. This may support the idea that surges end when peak water input reopens collapsed conduits, although it not clear why the first phase of the Bering Glacier surge lasted for over one year and terminated in the late-summer of 1994. It has been suggested by Harrison and others (1994), however, that the timing of surge termination in the cases of glaciers which advance at the terminus is not significant. The time of initiation at Bering Glacier casts some doubt on the notion that the timing of surges is controlled by the seasonal minima and maxima in meltwater input. The existence of a seasonal factor is supported by the multi-pulse surge which occurred at Bering Glacier because both events began at the same time of year. It may be possible that the large size of Bering Glacier results in a time lag between the beginning of conduit collapse and the build-up of enough basal water to cause accelerated sliding.

The observations of the progression of the Bering Glacier surge were consistent with the other observed surges summarized above, except for the manner of surge-front propagation. At Bering Glacier the surge front propagated down-glacier as a poorly-defined region of bulges and undulations in the ice surface. This may have been related to the much greater distance between valley walls, relative to most surge-type glaciers. The surge front at Bering Glacier was able to move out into the piedmont lobe without lateral constraint.

The outburst flood which apparently coincided with surge termination was also consistent with the behavior of other glacier surges, and it is the strongest indication of large volumes of stored subglacial water during the surge. This is consistent with the

hypothesis of fast ice motion caused by increased basal sliding, induced by high subglacial water pressure. Although there are no data pertaining to the amount of meltwater discharged from the glacier during the surge, the duration of the terminal flood and the apparent high sediment load suggest that the event may have been a near total discharge of water from beneath the portion of the glacier involved in the surge. The apparent high sediment load suggests that at least some of the bed is composed of sediment, rather than hard rock, but it is not possible to characterize the overall bed composition. The most curious aspect of the flood is that it occurred in the same location after both of the recent surge pulses, and also after the 1967 surge, as evidenced by similar morphologies seen in the aerial photographs of A. Post (personal communication). A possible explanation is that an unusually large channel or trough exists in the bed topography which collects most, if not all, of the subglacial drainage from Bering Glacier and carries it to one point of discharge. Preliminary data pertaining to the bed depth below sea level, collected by the U.S. Geological Survey, suggest that some kind of deep trough does exist in the general area up-glacier from the location of the flood (D. Trabant, personal communication).

The activity of Bering Glacier during its recent surge is consistent with the commonly accepted theory that elevated subglacial water pressure associated with basal water storage causes rapid sliding during a surge. The timing of surge onset shows fairly wide variation among different surge-type glaciers, and may imply a mechanism of initiation different from that suggested by Raymond (1987). The observed motion of the glacier during surge was consistent with observations of other surge-type glaciers. The

apparent termination of the surge at or near the time of the outburst flood was also consistent with other surging glaciers. The similarities between the surge behavior of Bering Glacier and other surge-type glaciers are particularly interesting because they suggest that the world's largest temperate glacier behaves in much the same way as many smaller surge-type glaciers.

Perhaps the greatest significance of this study, beyond its contribution to the body of knowledge on surging glaciers, is its demonstration of the utility of spaceborne SAR imagery for observation and measurement of glacier surges in remote regions. The clouds and darkness which frequently obscure the mountains of Alaska and the Yukon Territory, the short subpolar summers, and the expense and logistical difficulties of traditional field work make direct observation of surging glaciers difficult. The result is that few surging glaciers have been studied in detail. Application of SAR imagery to the study of surging glaciers can greatly expand our knowledge of these events because of the ease and frequency with which observations can be made. The problem of surging will not be solved without more field study, but satellite SAR imagery will aid in the detection of surge onsets and in reconnaissance measurements of glacier surges. That contribution shows promise of yielding progress toward a solution of the problem of surging glaciers.

### References Cited

Adam, S. 1995. Snow line mapping using radar imagery, Place Glacier, B.C. Masters thesis, Department of Geography, University of Saskatoon.

Alley, R.B., D.D. Blankenship, C.R. Bentley and S.T. Rooney. 1986. Deformation of till beneath ice stream B, West Antarctica. *Nature*, **323**, 57-59.

Bicknell, T. 1992. User's guide to products, Alaska SAR Facility Processor System. Jet Propulsion Laboratory Report JPL D-9362.

Bindschadler, R.A., K.C. Jezek and J. Crawford. 1987. Glaciological investigations using the synthetic aperture radar imaging system. *Annals of Glaciology*, **9**, 11-19.

Bindschadler, R.A. and P.L. Vornberger. 1994. Detailed elevation map of Ice Stream C, Antarctica, using satellite imagery and airborne radar. *Annals of Glaciology*, **20**, 327-335.

Blankenship, D.D., C.R. Bentley, S.T. Rooney and R.B. Alley. 1986. Seismic measurements reveal a saturated porous layer beneath an active Antarctic ice stream. *Nature*, **323**, 54-57.

Bush, S. 1991. Bering Glacier may be in retreat. *Eos* **72**(43), 466-467.

Clarke, G.K.C. 1991. Length, width and slope influences on glacier surging. *Journal of Glaciology*, **37**(126), 236-246.

Clarke, G.K.C., S.G. Collins and D.E. Thompson. 1984. Flow, thermal structure, and subglacial conditions of a surge-type glacier. *Canadian Journal of Earth Sciences*, **21**(2), 232-240.

Clarke, G.K.C., J.P. Schmok, C.S.L. Ommanney and S.G. Collins. 1986. Characteristics of surge-type glaciers. *Journal of Geophysical Research*, **91**(B7), 7165-7180.

Curlander, J. and R. McDonough. 1992. *Synthetic Aperture Radar: Systems and Signal Processing*. John Wiley and Sons, New York.

Dolgushin, L.D. and G.B. Osipova. 1975. Glacier surges and the problem of their forecasting. *International Association of Scientific Hydrology*, **104**, 292-304.

Dowdeswell, J.A., G.S. Hamilton and J.O. Hagen. 1991. The duration of the active phase on surge-type glaciers: contrasts between Svalbard and other regions. *Journal of Glaciology*, **37**(127), 388-400.

Echelmeyer, K.A., R. Butterfield and D. Cuillard. 1987. Some observations on a recent surge of Peters Glacier, Alaska, U.S.A. *Journal of Glaciology*, **33**(115), 341-345.

Fleisher, P.J., D.H. Cadwell, E.H. Muller and D.A. Franzi. 1990. Downwasting of Bering Glacier as an analog for New York glaciation. *Geological Society of America Abstracts with Programs*, **22**(2), 16.

Fleisher, P.J., E.H. Muller, D.H. Cadwell, C.L. Rosenfeld, A. Thatcher, and P.K. Bailey. 1994. Measured ice-front advance and other surge-related changes, Bering Glacier, Alaska, *Eos*, **75**(44), 63.

Fahnestock, M., R. Bindschadler, R. Kwok, and K. Jezek. 1993. Greenland ice sheet surface properties and ice dynamics from ERS-1 SAR imagery. *Science*, **262**, 1530-1534.

Fastook, J.L., H.H. Brecher, T.J. Hughes. 1995. Derived bedrock elevations, strain rates and stresses from measured surface elevations and velocities: Jakobshavns Isbrae, Greenland. *Journal of Glaciology*, **41**(137), 161-173.

Green, P.M. 1993. Bering Glacier summer research project: field trip and ice thickness estimation. Unpublished summer intern report, Geophysical Institute, University of Alaska Fairbanks.

Hall D.K. and J.P. Ormsby. 1983. Use of SEASAT synthetic aperture radar and LANDSAT multispectral scanner subsystem data for Alaskan glaciology studies. *Journal of Geophysical Research*, **88**(C3), 1597-1607.

Harrison, W.D., K.A. Echelmeyer, E.F. Chacho, C.F. Raymond and R.J. Benedict. 1994. The 1987-88 surge of West Fork Glacier, Susitna Basin, Alaska, U.S.A. *Journal of Glaciology*, **40**(135), 241-254.

Heinrichs, T.A., L.R. Mayo, D.C. Trabant and R.S. March. 1995. Observations of the surge-type Black Rapids Glacier, Alaska, during a quiescent period, 1970-92. U.S. Geological Survey Open-File Report 94-512.

Heinrichs, T.A., L.R. Mayo, K.A. Echelmeyer and W.D. Harrison. In press. Quiescent-phase evolution of a surge-type glacier: Black Rapids Glacier, Alaska, U.S.A. *Journal of Glaciology*.

Herzfeld, U.C., C.S. Lingle, and L.-h. Lee. 1993. Geostatistical evaluation of satellite radar altimetry for high resolution mapping of Lambert Glacier, Antarctica. *Annals of Glaciology*, **17**, 77-85.

Jezek, K.C., M.R. Drinkwater, J.P. Crawford, R. Bindshadler and R. Kwok. 1993. Analysis of synthetic aperture radar data collected over southwestern Greenland ice sheet. *Journal of Glaciology*, **39**(131), 19-32.

Kamb, B.C. 1987. Glacier surge mechanism based on linked cavity configuration of the basal water conduit system. *Journal of Geophysical Research*, **92**(B9), 9083-9100.

Kamb, B.C., C.F. Raymond, W.D. Harrison, H. Engelhardt, K.A. Echelmeyer, N. Humphrey, M.M. Brugman and T. Pfeffer. 1985. Glacier surge mechanism: 1982-1983 surge of Variegated Glacier, Alaska. *Science*, **227**(4686), 469-479.

Lingle, C.S., A. Post, U.C. Herzfeld, B.F. Molnia, R.M. Krimmel and J.J. Roush. 1994. Bering Glacier surge and iceberg-calving mechanism at Vitus Lake, Alaska, U.S.A. *Journal of Glaciology*, **39**(133), 722-727.

Logan, T. 1994. Terrain correction of synthetic aperture radar imagery using the Cray T3D parallel processor. Masters thesis. Computer Sciences, University of Alaska Fairbanks.

Maddren, A.G. 1914. Mineral deposits of the Yakataga District. U.S. Geological Survey Bulletin 592, 119-153.

Martin, G.C. 1908. The petroleum fields of the Pacific coast of a Alaska with an account of the Bering River coal deposits. U.S. Geological Survey Bulletin 250.

Meier, M.F. and A. Post. 1969. What are glacier surges? *Canadian Journal of Earth Sciences*, **6**(4), 807-817.

Meier, M.F. and A. Post. 1987 Fast tidewater glaciers. *Journal of Geophysical Research*, **92**(B9), 9051-9058.

Miller, D.J. 1961. Geology of the Yakataga District, Gulf of Alaska Tertiary Province, Alaska. U.S. Geological Survey Open File Report, 2 sheets.

Molnia, B.F., D.C. Trabant, A. Post and D.G. Frank. 1990. Bering Glacier, Alaska: factors influencing the potential for irreversible calving retreat (abstract only). *Eos*, **71**(43), 1314.

Molnia, B.F. and D.C. Trabant. 1992. Ice-thickness measurements on Bering Glacier, Alaska and their relation to satellite and airborne SAR image patterns. *Eos*, **73**(43), 181.

Molnia, B.F. 1993. Major surge of the Bering Glacier. *Eos*, **74**(29), 321-322.

Molnia, B.F., and A. Post. 1995. Holocene history of Bering Glacier, Alaska: a prelude to the 1993-94 surge. *Physical Geography*, **16**(2), 87-117.

Muller, E.H., A. Post, P.J. Fleisher and C.J. Heusser. Unpublished manuscript. Late Holocene Stratigraphy, glacial fluctuations and surging history at the east margin of Bering Glacier's piedmont lobe.

Muller, E.H. and P.J. Fleisher. 1995. Surging history and potential for renewed retreat: Bering Glacier, Alaska, U.S.A. *Arctic and Alpine Research*, **27**(1), 81-88.

Olmsted, C. 1993. Alaska SAR Facility scientific SAR user's guide. Alaska SAR Facility Report ASF-SD-003.

Paterson, W.S.B. 1994. *The Physics of Glaciers. Third Edition*. Oxford, Pergamon Press.

Pierce, R.A. and J.H. Winslow. 1979. *HMS Sulphur on the Northwest and California coasts, 1837 and 1839: the accounts of Captain Edward Belcher and Midshipman Francis Guillemard Simpkinson*. The Limestone Press, Kingston.

Post, A. 1969. Distribution of surging glaciers in western North America. *Journal of Glaciology*, **8**(53), 229-240.

Post, A. 1972. Periodic surge origin of folded medial moraines on Bering Piedmont Glacier, Alaska. *Journal of Glaciology*, **11**(62), 219-226.

Raymond, C. 1987. How do glaciers surge? A review. *Journal of Geophysical Research*, **92**(B9), 9121-9134.

Rott, H. and C. Matzler. 1987. Possibilities and limits of synthetic aperture radar for snow and glacier surveying. *Annals of Glaciology*, **9**, 195-199.

Roush, J.J., C.S. Lingle and R.M. Guritz. 1994, submitted. The surge of Bering Glacier, Alaska, observed with satellite synthetic aperture radar. *Journal of Glaciology*.

Shabtaie, S., I.M. Whillans and C.R. Bentley. 1987. The morphology of ice streams A, B, and C, West Antarctica, and their environs. *Journal of Geophysical Research*, **92**(B9), 8865-8883.

Trabant, D.C., B.F. Molnia and A. Post. 1991. Bering Glacier, Alaska--Bed configuration and potential for calving retreat. *Eos*, **72**(44), 159.

U.S. Geological Survey. 1990. Digital elevation models: Data users guide 5. National Mapping Program Technical Instructions.